SANDIA REPORT

SAND2000-0821
Unlimited Release
Printed April 2000

Silicon Purification Melting for Photovoltaic Applications

James Van Den Avyle, Pauline Ho, and James M. Gee

Prepared by
Sandia National Laboratories
Albuquerque, New Mexico 87185 and Livermore, California 94550

Sandia is a multiprogram laboratory operated by Sandia Corporation, a Lockheed Martin Company, for the United States Department of Energy under Contract DE-AC04-94AL85000.

Sandia National Laboratories

Issued by Sandia National Laboratories, operated for the United States Department of Energy by Sandia Corporation.

Available to DOE and DOE contractors from
Office of Scientific and Technical Information
P.O. Box 62
Oak Ridge, TN 37831

Prices available from (703) 605-6000
Web site: http://www.ntis.gov/ordering.htm

Available to the public from
National Technical Information Service
U.S. Department of Commerce
5285 Port Royal Rd
Springfield, VA 22161

DISCLAIMER

DISCLAIMER

Portions of this document may be illegible in electronic image products. Images are produced from the best available original document.

SAND 2000-0821
Unlimited Release
Printed April 2000

Silicon Purification Melting for Photovoltaic Applications

James Van Den Avyle
Mechanical Reliability and Melting Department

Pauline Ho
Chemical Processing Science Department

James M. Gee
PV Systems Components Department

Sandia National Laboratories
P. O. Box 5800
Albuquerque, NM 87085-1134

Abstract

This work investigates the thermochemical treatment of metallurgical grade silicon to reduce impurities to a low level suitable for use in photovoltaic applications. The first section of this report describes experiments in a vacuum induction furnace to purify bulk quantities of molten silicon using a combination of evaporation in vacuum and reaction with ammonia gas. This approach resulted in partial removal of some impurities, but the long reaction times were impractical and inefficient for this type of furnace. The second section of this report presents data and results from chemical equilibrium calculations that examine the likely effectiveness of various "gas blowing" treatments to remove aluminum impurities from polysilicon melts.

Acknowledgements

The authors acknowledge the expertise of Dr. Frank Zanner who played an important role in starting this project through his early research in 1982; he was also an active participant in conducting the experiments reported here. We also thank Drs. James Stepanek and Rodney Williamson who contributed experimentally and with thermodynamic modeling. James Maroone, Michael Baldwin, and Mark Miszkiel also made important contributions to running the experiments.

This work was funded by the Sandia National Laboratories' Laboratory Directed Research and Development (LDRD) Program as part of a project entitled "Solar-Grade Polysilicon Development."

Table of Contents

List of Figures

List of Tables

Silicon Purification Melting for Photovoltaic Applications

I. Introduction

The availability of polysilicon feedstock has become a major issue for the photovoltaic (PV) industry in recent years. Most of the current polysilicon feedstock is derived from rejected material from the semiconductor industry. However, the reject material can become scarce and more expensive during periods of expansion in the integrated-circuit industry. Continued rapid expansion of the PV crystalline-silicon industry will eventually require a dedicated supply of polysilicon feedstock to produce solar cells at lower costs.

The photovoltaic industry can accept a lower purity polysilicon feedstock ("solar-grade") compared to the semiconductor industry. The purity requirements and potential production techniques for solar-grade polysilicon have been reviewed [1]. One interesting process from previous research involves reactive gas blowing of the molten silicon charge. As an example, Dosaj *et alia* reported a reduction of metal and boron impurities from silicon melts using reactive gas blowing with O_2 and Cl_2 [2]. The same authors later reassessed their data and the literature, and concluded that Cl_2 and O_2/Cl_2 gas blowing are only effective for removing Al, Ca, and Mg from the silicon melt [3]. Researchers from Kawasaki Steel Corp. reported removal of B and C from silicon melts using reactive gas blowing with an O_2/Ar plasma torch [4]. Processes that purify the silicon melt are believed to be potentially much lower cost compared to present production methods that purify gas species.

One potential source of inexpensive silicon is metallurgical grade (MG) silicon, which typically contains 0.1-0.5 wt.% total impurities. This material is used in large quantities for steel making, and sells currently for approximately $2/kg. For the MG Si to be purified up to solar grade (SoG), impurities such as B, P, Fe, Ca, Ti, Al, C, and Na must be removed to levels well below ~1 ppma, with the metallic species well below 0.001 ppm.

With molten metal metallurgical processing there are four potential purification steps that could be utilized: 1) vacuum treatment to evaporate some elements, 2) treatment with reactive gases to

react with the other elements, 3) treatment with a molten slag to react directly with impurities or to remove solid reaction byproducts resulting from gas treatments, 4) followed by directional solidification of the product to further remove impurities which segregate during solidification, The experimental work described in Section II of this report deals with the first three steps.

Thermodynamic modeling provides important guidance toward favorable physical processes and chemical reactions to remove impurities, as well as optimum operating temperatures and pressures. These models have developed to a level where they can incorporate a large number of reacting elements and compounds. Reference 5 contains a description of the problem, calculational methods, and results for removal of C, B, P and Fe impurities from molten Si. Section III below is a supplement which provides data and results for Al removal. Thermodynamic models do not, of course, predict the rates of processes; measuring these rates was one of the goals of the experimental work below.

II. Melt Processing Experiments to Purify Metallurgical Grade Silicon

Investigations into the purification of metallurgical grade silicon by high temperature melt processing were performed at the Liquid Metals Processing Laboratory (LMPL) at Sandia National Laboratories. This process involved the injection of gasses into (or onto) a molten silicon bath and was designed to remove undesirable elements through formation of solid or gaseous reaction products. Initial consultation with thermodynamic data, relevant literature, and computer modeling suggested favorable gas species; these included oxygen, nitrogen, ammonia, water vapor, and HCl (as well as gaseous Cl_2 and other chlorine compounds) [5]. A significant effort to utilize moist argon as a reacting gas mixture is already successfully underway at Crystal Systems, Inc. under the DOE's Photovoltaic Manufacturing Technology (PVMaT) project. The chlorine-bearing species were deemed too corrosive for the LMPL furnace and its associated vacuum pumping system.

Experiments at Sandia were focussed on a combination of vacuum exposure plus reacting the molten Si with ammonia (NH_3) gas. Modeling suggests that P, Al, and Fe should physically volatize from the melt under vacuum. Ammonia heterogeneously dissociates at high

temperatures, so an NH_3 gas stream blown onto the molten Si surface or bubbled into Si should dissociate on contact with the Si and thereby provide N atoms for dissolution into the melt. Thermodynamic modeling [5] shows that reactions of N with B, Al, P, and Ti are favorable. N combines with P to form volatile PN. B, Ti, and Al combine with N to form solid nitrides. In particular, the possible reaction with B is important since directional solidification is incapable of removing it. The gaseous products should escape into the vacuum chamber and either be trapped on cooler solid surfaces or be pumped out. Solid nitrides need to be trapped in a molten slag or on the crucible walls. It is also useful in that the impurities in question are much more reactive with nitrogen than silicon, thus minimizing yield loss.

A. Experimental Design and Procedure

Silicon melting experiments were run in a 175 kW vacuum induction melting furnace with an internal volume of 11 m^3 which was pumped for these experiments by a Stokes 1722 vacuum pumping station rated at 2000 m^3/min. This furnace is configured with the induction coil box mounted on the door to allow tilt pouring into a mold within the chamber (Figure 1). On the top lid of the furnace are visual viewports, an optical pyrometer temperature sensor, and a material insertion vacuum port. This port was used during the melts to take samples, add material to the crucible, and to insert a gas flow lance. Data logged during each experiment included furnace power, vacuum level, molten Si temperature, and gas flow. The molten Si surface temperature was monitored using an optical pyrometer.

Since solid Si is not very conductive, a graphite susceptor is required to heat the Si charge; heating of the Si is then done by conduction and radiation from the graphite until the Si melts and conducts current. Several susceptor/crucible designs were tested in the course of these experiments with the goal of getting more rapid and efficient thermal coupling. Earlier melts used a graphite crucible coated with yttria on the interior, but to minimize reaction with the crucible and decrease contamination, a 30 cm diameter by 25 cm high quartz silica crucible was chosen to contain the molten silicon. This added crucible also slowed the heating rate. Figure 2 shows an intermediate box design with a vertical split ring graphite susceptor placed between the crucible and the induction coils. In between the graphite and the crucible was packed a thin layer

(6 mm) of silica sand. It was also packed between the crucible and the magnesia furnace liner on the bottom so that upon expansion of the silicon with freezing, the sand could give, and the furnace would not be damaged.

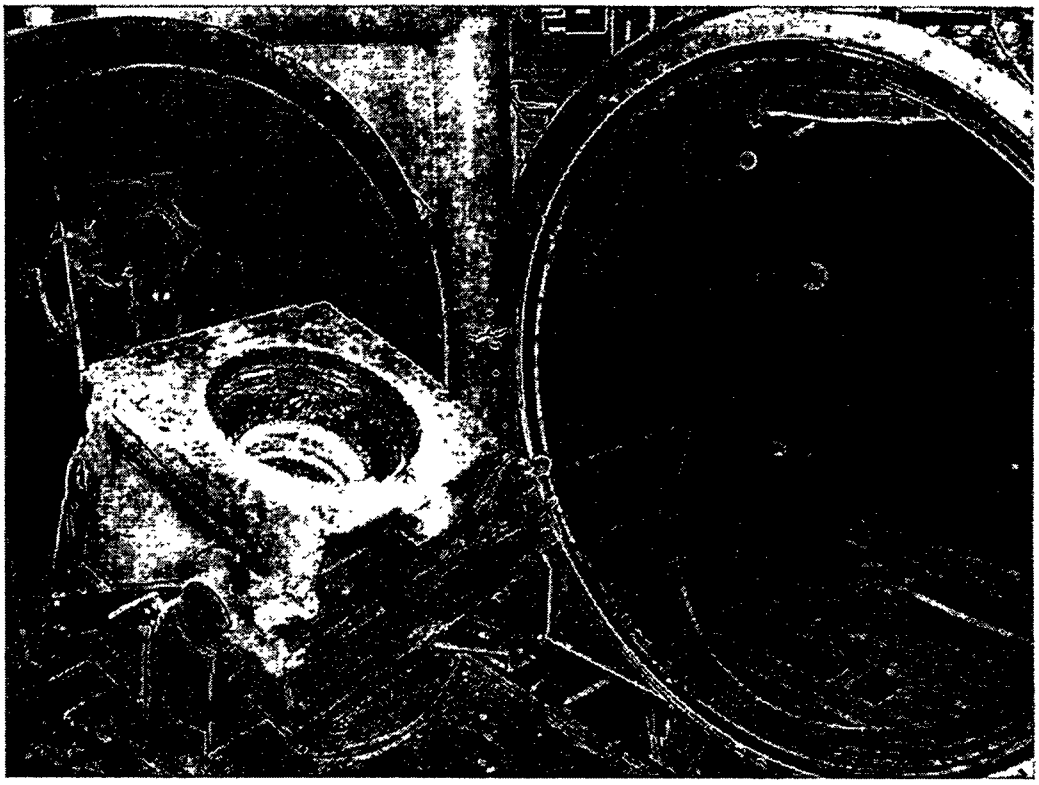

Figure 1. Furnace door opened to show the door-mounted tilt pour induction crucible after a melting experiment. Top of box and crucible are covered with silica deposits.

MG silicon in this experiment was purchased from Globe Metallurgical Inc. (supplier specifications of 99.58% Si, 0.015 Ca, 0.094 Fe) at a cost of $2/kg for 700 kg. This material was roughly sized as 10 cm chunks (Figure 3). Some pieces were contaminated with slag on one surface, others had veins of slag running through them. This slag was analyzed as primarily silica. The pieces were presorted for the experiments to eliminate pieces with significant slag within the piece. Pieces were sand blasted to remove any surface slag. A maximum 45 kg MG Si sample charge could be dense-stacked to the top of the crucible. Experience showed that the top of this stack would not easily melt in due to inefficient heating and high heat loss at the top. Final melts were conducted with 20.5 kg of Si.

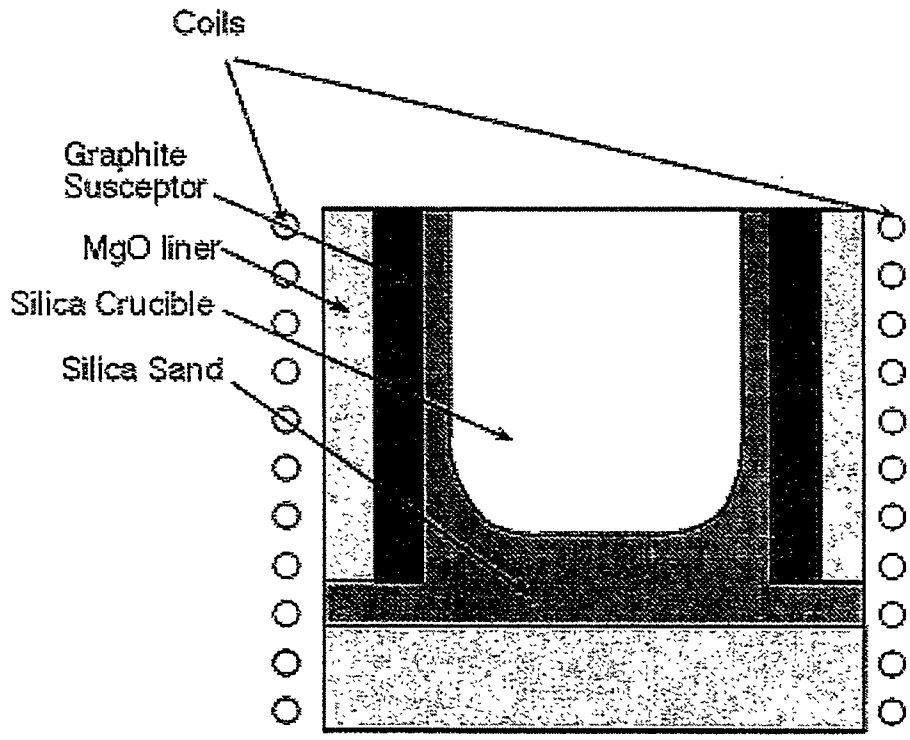

Figure 2. Schematic drawing of induction heating box with split ring graphite susceptor.

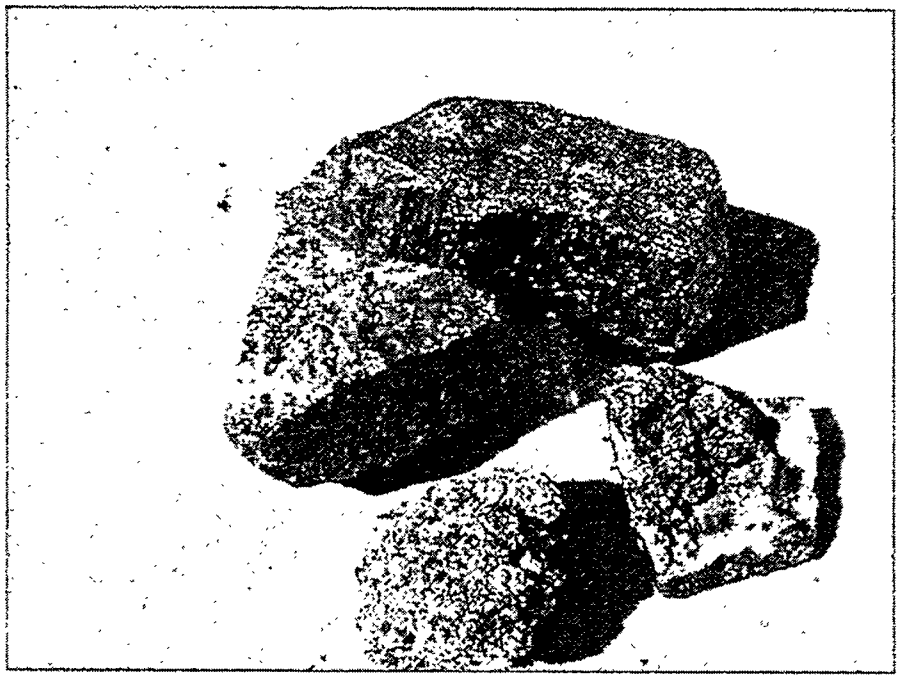

Figure 3. Metallurgical grade silicon melt stock; the two smaller bottom pieces contain considerable slag and would be discarded.

Gas was introduced to the melt through a quartz tube attached to a water-cooled lance. In initial tests the tube tip was submerged below the molten Si surface to attempt to bubble the gas. The violence of the gas expansion at this temperature, even at low flow rates, caused extreme spatter and precluded this approach. Given the high level of stirring which is evident during the melts due to the inductive stirring, it was concluded that surface blowing would be sufficient to expose silicon surface area to the gas. Experiments were conducted using Ar, N_2, NH_3, and air injection. The lance tip was inserted to approximately 5 cm above the liquid, and gas flow was adjusted to give a maximum depression in the liquid Si without spattering (Figure 4).

Two methods of sampling were used. The first used a large copper dipping block with a hemispherical depression to collect the liquid Si (Figure 5). It was expected that its large thermal mass would chill the sample before reactions could take place; in one case the stainless steel bolts holding the sampler together partially melted, so a quartz dip tube was also tested.

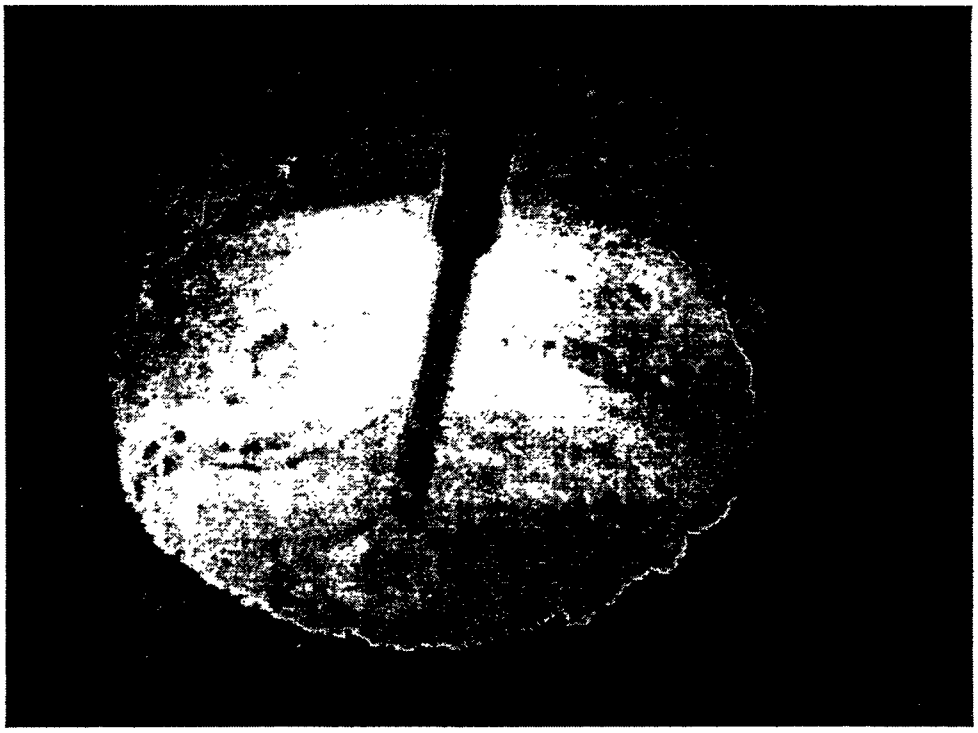

Figure 4. Blowing NH_3 through quartz tube onto molten Si. Deposits on tube and crucible lip are a mixture of Si spatter and oxides of Si.

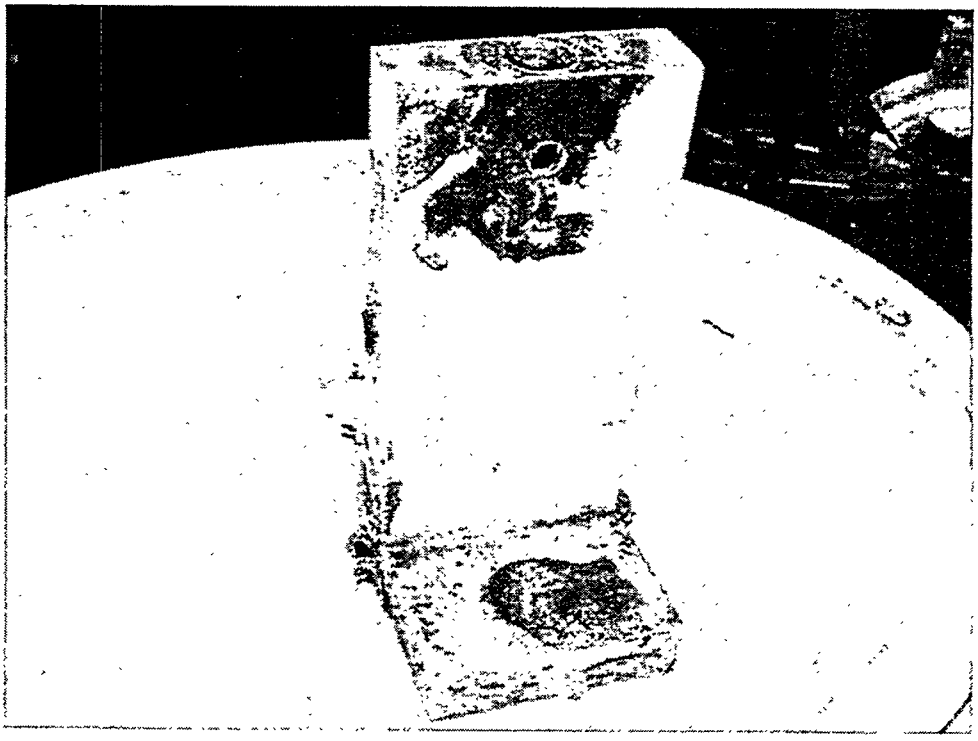

Figure 5. Copper dip sampler after use. Si is sample at bottom, and white deposits are Si oxides deposited during the brief dipping exposure.

B. Results

Several initial trial melts were conducted to develop the experimental process, including crucible configuration, gas blowing system, sampling methods, and techniques to add Si or other materials to the melt. An important potential advantage of induction heating is that the melt is very well stirred by the induced fields. This stirring also aids in melting the charge since the moving fluid transfers heat from the crucible wall to the solid.

Attempts to add slag to the molten Si and blow with gas were not successful. A 1.5 kg slag addition of powdered lime- magnesia- silica- titanium dioxide was dropped onto the melt. It reacted with the Si, and some of the slag powder was ejected from the melt. The remainder melted and floated on top of the melt, but the reaction continued with gas generation. This was likely due to reaction of the SiO_2 in the slag with Si to form gaseous SiO. The SiO_2 was added to the slag mixture to promote fluidity, so as it was removed, the slag became much more viscous. This occurred over several minutes, and the viscous slag layer interfered with gas flow to the Si surface.

The following two experiments evaluated vacuum exposures and gas treatment to purify MG Si:

Silicon Melt V338

The purpose of this experiment was to expose molten Si to 30 min of vacuum followed by 30 min. of blowing with NH_3. The crucible was charged with 20.2 kg of MG silicon. To begin the experiment the furnace was pumped down and a leak rate of 65 mtorr/ hr was achieved. The power was turned on to the induction coils at 10:00 AM. The procedure is listed in Table 1.

Table 1. History of experiment V338

Time	Power (kW)	Temperature (°C)	Pressure (mtorr)	Comment
10:00	20		21.4	
10:15	30		22.9	
10:25	40		49.7	
10:40	50		133	
10:50	60		139	
11:54	80		119	
12:20	80		159	Si turning red
12:42	Off		190	White hot spot
13:10	80		177	
14:00	90		207	
14:25	92		230	
14:35	100		229	
14:55	60		256	Melted in
15:24	20		235	Lance in/no gas
15:26	20		231	
15:28	20	1550	750	Gas on
15:31	40		840	
15:50	42		868	
15:56	42		870	Gas off
15:58	Off			Left to solidify in crucible

Melt-in took five hours, a long period caused by the inefficient thermal transfer of this crucible/susceptor design. During melt-in, white hot spots developed at the segment joints in the graphite susceptor. This was due to electrical arcing between the graphite segments. This

produced vapor or gas bursts at those locations and ejected quantities of the packing sand (silica of unknown purity) at those sites. Some of the ejected material contaminated the melt.

Some other details are not covered in the table. A significant amount of gas bubbling and spitting was observed during the initial melting of the Si charge. This was likely caused by Si reaction with silica impurities (slag) still present with the solid feed stock to produce gaseous SiO. This reaction subsided after 10-15 min. melting. During the melt a section of solid silicon bridged the top of the crucible and failed to melt in. This was despite very vigorous agitation of the melt from induction stirring. An attempt was made to break this bridge, but this appeared to damage the crucible so it was stopped. Owing to this bridge, it was apparent that the sample cup would not be able to fit into the molten area of the silicon. It was decided that the melt should be allowed to solidify in place and a final sample taken from the solid remaining in the crucible. During removal of the lance from the furnace chamber, the silica tube broke off and fell onto the melt. This was not perceived to be a problem, as it stayed on the top of the solid bridge on the melt.

After the Si ingot was solidified, it was removed from the furnace. Upon removal it was observed that the silica crucible had cracked during the normal expansion of silicon during solidification; no silicon flowed onto the solid top of the ingot to relieve pressure. Some liquid silicon leaked into the sand packing and reacted with the graphite. Three samples were broken off the ingot and were sent for analysis (to Northern Analytical Laboratory, Merrimack, NH), along with four samples of slag-free, as-received MG silicon. These results are reported in Table 2 below. It can be seen that significant reductions of Al and Ti, and others were accomplished. B was minimally affected, and P was marginally reduced; modeling had predicted that these species could be affected by this processing technique. Other elements significantly reduced were C, Mg, Ca, V, Cr, Mn, Fe, Co, Ni, Cu, Zr. The data also show significant sample to sample variations in some elements for both the as-received MG-Si and the treated Si.

Given the short time (28 min.) of gas processing in this experiment, the effects on some of the species were minimal. Boron removal is likely to take a longer time, and phosphorus removal requires longer vacuum exposure time in a hard vacuum.

Table 2. Analyses of as-received MG silicon and samples from melt V338

Element (ppm)	MG1	MG2	MG3	MG4	3/3/99D	3/3/99F	3/3/99A
Li	0.016	0.03	0.019	0.053	0.012	0.016	0.017
B	32	28	37	23	25	24	24
C	90	80	100	1200	43	27	26
Na	0.036	0.024	0.014	0.074	0.014	0.011	0.03
Mg	25	9.5	17	1.7	0.064	0.13	0.012
Al	125	35	70	140	6.5	12	2.4
P	34	21	35	16	14	16	19
S	0.076	0.054	0.051	0.56	0.084	0.08	0.036
Cl	0.56	0.43	0.48	0.92	0.55	0.5	0.43
K	0.025	0.13	0.47	0.52	0.027	0.031	0.073
Ca	60	30	31	50	3.2	2.5	0.48
Ti	60	25	39	50	1.5	4.2	0.27
V	3.6	1.5	2.7	3.8	0.14	0.34	0.017
Cr	33	13	22	46	0.25	1	0.025
Mn	54	18	33	62	0.77	4.5	0.15
Fe	2305	920	1500	3200	25	150	4.7
Co	4.8	1.8	3.8	3.5	0.066	0.36	0.008
Ni	9.4	3.2	5.3	8.3	0.091	0.53	0.052
Cu	14	3.9	8.1	12	0.26	1.6	0.15
Zn	0.05	0.05	0.05	0.38	0.05	0.05	<0.05
Ge	5.7	2.7	7	3.9	2.9	5.1	2.1
As	0.42	0.19	0.42	0.48	0.12	0.26	0.11
Zr	3.8	1.8	2.9	1.1	0.11	0.36	0.02
Mo	1	0.55	0.7	0.81	0.033	0.1	0.015
Ba	0.45	0.23	0.19	0.47	0.06	0.018	0.013
La	3.5	1.5	1.7	2.2	0.13	0.38	0.027
Ce	6.5	2.7	3.1	4.3	0.33	0.66	0.68
Pr	0.8	0.32	0.37	0.56	0.05	0.086	0.14
Nd	2.2	0.85	1	1.5	11	0.22	0.05
W	0.41	0.26	0.23	0.39	0.049	0.048	0.025
Th	0.15	0.07	0.069	0.074	0.01	0.024	0.01
U	0.24	0.086	0.15	0.12	0.01	0.022	0.01

As can been seen in Table 2, melting the silicon metal took five hours, a long time for induction melting. This was due to poor heat transfer from the graphite susceptor to the silica crucible and poor susception of the split graphite ring. Also, the bridging that was evident in the melt showed

that heat losses out the top due to radiation were quite severe, and more heat input at the top surface was necessary. A new crucible/susceptor was designed for the next experiment to compensate for this .

Silicon Melt V339

This experiment was designed to process the molten Si in two stages. The crucible was charged with 20.2 kg of MG silicon and melted in the vacuum induction furnace. The first treatment stage was vacuum exposure for approximately one hour to assess evaporation of phosphorus from the melt. The second stage was a two-hour ammonia gas blow to evaluate removal of boron and other impurities.

Learning from the problems found in the prior experimental run, a new crucible and susceptor arrangement was employed in V339. The design is shown in Figure 6 below. It places the crucible down lower into the induction coils, with greater susceptor area available above it for radiative heat input. Also the susceptor is one-piece construction, covering the bottom of the crucible to heat that area as well. This one-piece construction also eliminates the chance of arcing between segments.

The ammonia gas was injected using a quartz silica tube attached to a water-cooled lance. Gas was injected onto the surface only. The quartz tube was positioned approximately 5 cm above the melt surface, and the gas flow was adjusted to produce a steady state furnace pressure below 800 mtorr (to avoid plasma arcing in the furnace induction coils). This gas flow produced a dimple on the liquid Si surface without causing spatter.

A new sampling method was attempted using a 1 cm ID straight quartz silica tube, but on the first attempt it was found that an insufficient amount of silicon remained in the tube upon dipping, and the copper dip samplers were used instead. Two samples were taken from the melt using a copper dip apparatus, which would chill the sample due to thermal mass before reactions could take place. A total of three samples were analyzed: one from half way through the vacuum treatment, after one-half hour of ammonia treatment, and from the solidified ingot.

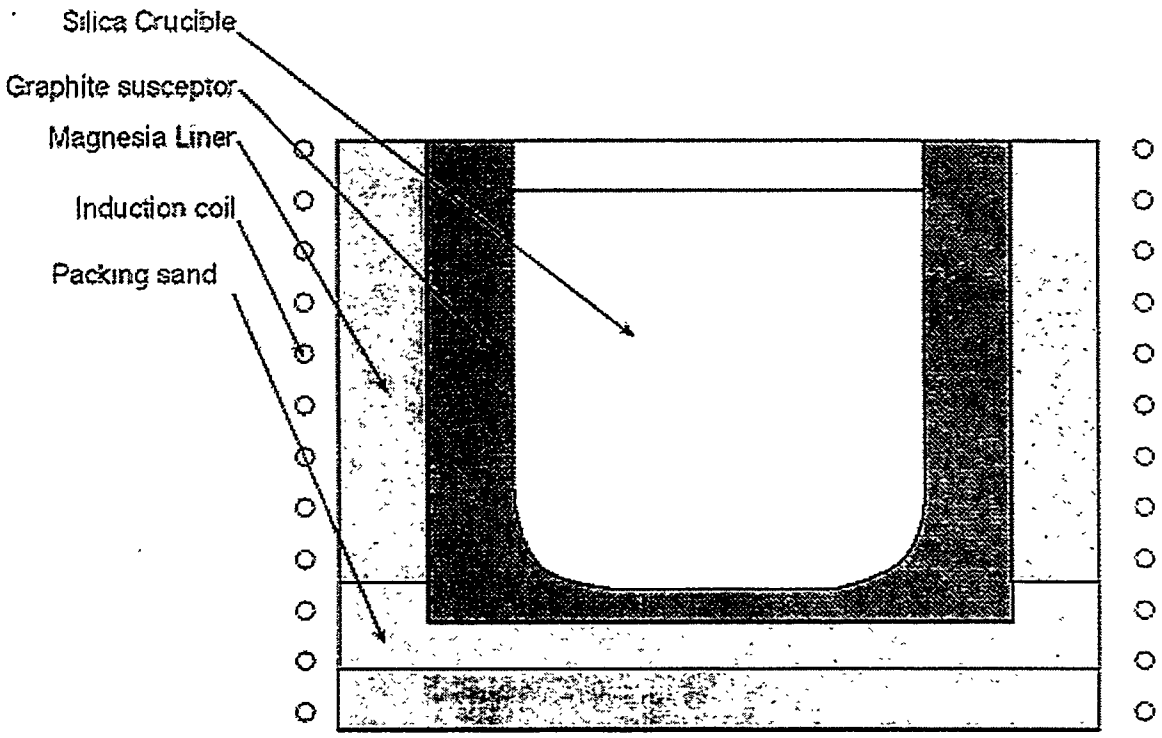

Figure 6. Revised crucible and susceptor design in vacuum induction furnace; a thin layer of silica sand was placed between the crucible and susceptor to allow relative motion.

Prior to the experiment, the crucible/ susceptor apparatus was baked out (at 1330°C) in the furnace to remove volatile organic components and moisture. To begin the experiment, the furnace was pumped down, and a leak rate of 14 mtorr/ hr was achieved. The power was turned on to the induction coils at 8:17 AM. The procedure went as follows:

Table 3. History of experiment V339

Time	Power (kW)	Temperature (°C)	Pressure (mtorr)	Comment
8:17	20		6.8	
8:37	30		7.4	
8:50	40		10.3	
9:00	50		17.9	
9:10	75		31.6	
9:20	100		52.5	
9:31	100		122	

9:33	100		152.5	Si dull red
9:38	100		240	
9:41	100		279	
9:43	100		299	
9:46	100	1180	329	
9:50	100	1202	353	
9:52	100	1223	362	
9:55	100	1257	368	Melting below
10:00	100	1294	371	
10:02	100	1282	370	Si dropping in
10:10	100	1410	390	melted, vigorous bubbling
10:11	80		389	
10:12	50	1493	380	All melted
10:17		1527	359	Bubbling
10:18	40	1538	374	
10:19	30	1540	365	Violent bubbling
10:20	15	1568	345	"
10:21	15	1527	325	"
10:24	15	1557	286	"
10:30	15	1516	237	Bath quiet
10:31	15	1521		"
10:36	20		218	
10:37	20	1477		Failed silica tube sample
10:42	30		216	Dendrite growth from side
11:00	60		252	Frozen over
11:20	55		271	Starting to melt in
11:25	30	1443		Violent bubbling, solid skin melting
11:26	35			
11:27	40			
11:28	38			
11:29	38	1476	281	All remelted
11:30		1510		Sample 1
11:31	34	1496	280	
11:34		1499		
11:36	34	1499	274	
11:39	39		280	Starting to freeze in from edge
11:41	39	1493		
11:45	43	1489	325	
11:46	48		315	Start ammonia flow
11:47	42		443	
11:48	42		593	Tube 5 cm above surface
11:51	50	1482	685	Ammonia flow rate equivalent to 1.4 m^3/ hr of Ar
11:55	50	1493	710	

11:58	45	1493	725	
12:03	45	1498	695	
12:11				Furnace tilted, broke silica gas injection tube
12:15	40	1488	155	Bath quiescent , readying sample dip
12:16				Sample 2
12:36	45		515	Resume ammonia flow
12:52	45		638	
12:53	40		637	
13:03	40		661	
13:08	40		676	Bubbles emerging from center of melt (where silica lance fell)
13:30	50		698	Skin developing
1:46	50		717	Larger skin
1:53	40		500	Gas off
1:54			310	Power off

The above table comprehensively covers the details of the melt. The modified susceptor design was thermally more efficient and reduced the melt-in time for the Si charge to less than two hours. The pre-melt bakeout procedure for the crucible/susceptor assembly did not reduce the furnace pressure during the vacuum treatment compared to the earlier melt. A gas generating reaction was observed between the Si melt and the silica crucible when the melt temperature exceeded 1525°C. The bubbling is thought to be due to the evolution of silicon monoxide. At lower temperatures gas was not generated, and the molten Si was rapidly circulated by induction stirring. The center bubbling which occurred later in the melt is assumed to be a product of reaction with the broken silica tube. The SiO deposited on cooler surfaces within the furnace to form a white or tan deposit (see Figures 1 and 7).

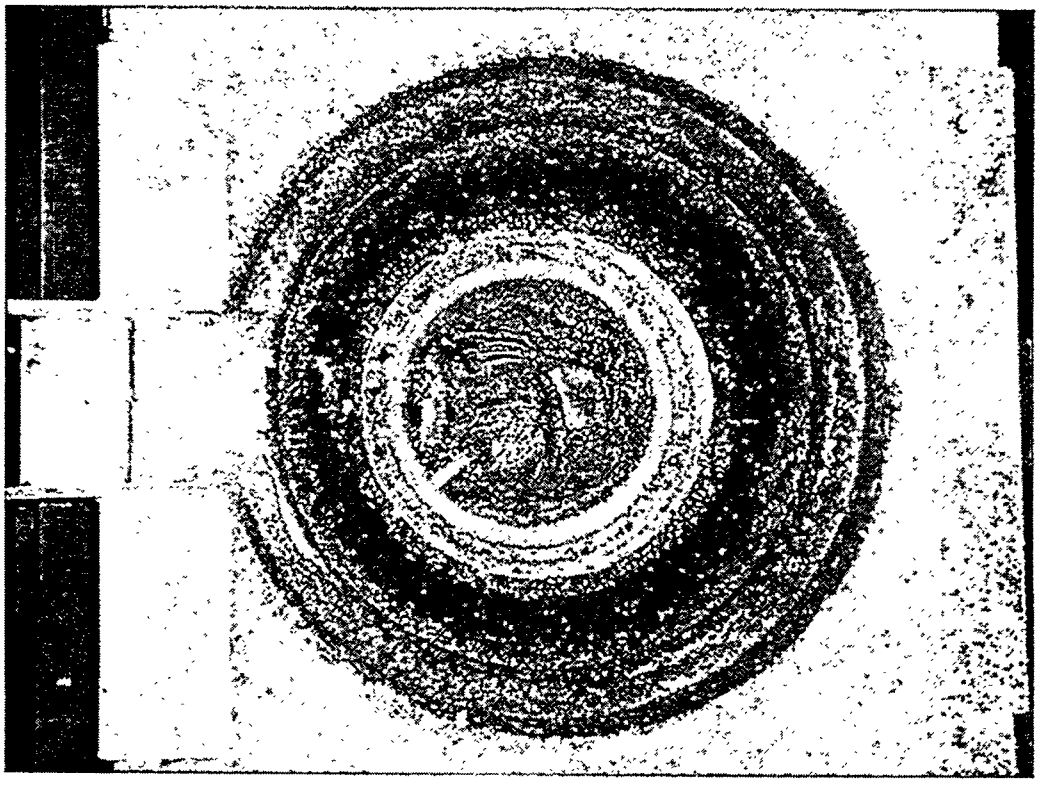

Figure 7. Top of crucible and susceptor after melting showing silica deposits

After the ingot was solidified, it was removed from the furnace (Figure 8). The silica crucible again cracked during the expansion due to solidification. This expansion also managed to crack the graphite susceptor. The silica sand put between the crucible and susceptor was melted or densified, and it did not act to relieve thermal strains during cooldown. The Si ingot was also highly fissured. Samples were broken off the ingot and were sent for chemical analysis. These results are reported in Table 4, along with results from the samples of as-received MG silicon.

Levels of P decreased by roughly a factor of two after the first 0.5 hr of vacuum treatment and did not decrease with additional time in the furnace (Figure 9); this was the same level of reduction as the shorter exposure melt V338. B levels did not appear to systematically change during the experiment. Ti, Al, and Ca levels also decreased by a factor of two or more (Figure 10). A number of other elements, C, Mg, V, Mn, Fe, Co, Cu, and Zr, were also significantly reduced (Table 4). Cr and Ni levels decreased prior to the final ingot sample (Figure 11), where the increased values are likely due to dissolution of the stainless steel bolt on the copper dipper

used to take the previous sample. There was no apparent Cu contamination of the melt caused by the sample dipper. The data also show significant sample to sample variations in some elements for both the as-received MG-Si and the treated Si.

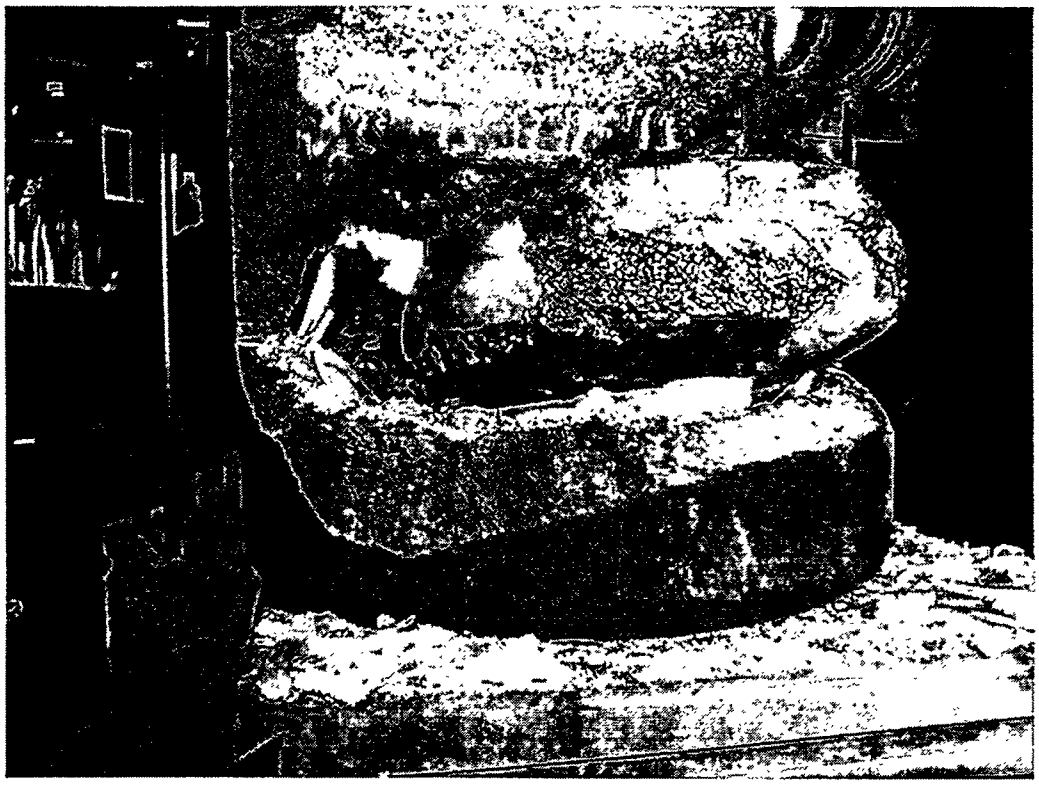

Figure 8. Silicon ingot produced in melt V339 removed from fractured quartz silica crucible and graphite susceptor

Table 4. Analyses of as-received MG silicon and samples from melt V339

Element (ppm)	MG1	MG2	MG3	MG4	4/27/99-1	4/27/99-2	4/27/99-3
Li	0.016	0.03	0.019	0.053	0.017	0.015	0.12
B	32	28	37	23	37	22	26
C	90	80	100	1200	55	70	36
Na	0.036	0.024	0.014	0.074	0.044	0.016	0.014
Mg	25	9.5	17	1.7	0.17	0.10	0.015
Al	125	35	70	140	68	29	31
P	34	21	35	16	13	14	11
S	0.076	0.054	0.051	0.56	0.059	0.15	0.065
Cl	0.56	0.43	0.48	0.92	0.060	0.80	0.40
K	0.025	0.13	0.47	0.52	0.10	0.28	0.081
Ca	60	30	31	50	0.19	16	21
Ti	60	25	39	50	3.8	7.6	5.2
V	3.6	1.5	2.7	3.8	0.42	0.45	0.49
Cr	33	13	22	46	9.4	4.3	27
Mn	54	18	33	62	18	9.0	14
Fe	2305	920	1500	3200	505	550	525
Co	4.8	1.8	3.8	3.5	0.57	0.45	0.62
Ni	9.4	3.2	5.3	8.3	2.2	1.3	11
Cu	14	3.9	8.1	12	4.7	2.6	4.9
Zn	0.05	0.05	0.05	0.38	0.19	0.30	0.21
Ge	5.7	2.7	7	3.9	4.0	2.8	4.5
As	0.42	0.19	0.42	0.48	0.13	0.44	0.29
Zr	3.8	1.8	2.9	1.1	0.31	0.47	0.38
Mo	1	0.55	0.7	0.81	0.18	0.50	0.58
Ba	0.45	0.23	0.19	0.47	0.095	0.16	0.11
La	3.5	1.5	1.7	2.2	0.14	0.55	0.23
Ce	6.5	2.7	3.1	4.3	0.17	1.1	0.32
Pr	0.8	0.32	0.37	0.56	0.040	0.12	0.05
Nd	2.2	0.85	1	1.5	0.040	0.36	0.18
W	0.41	0.26	0.23	0.39	0.10	0.12	0.11
Th	0.15	0.07	0.069	0.074	<0.01	0.10	<0.01
U	0.24	0.086	0.15	0.12	<0.01	0.30	0.013

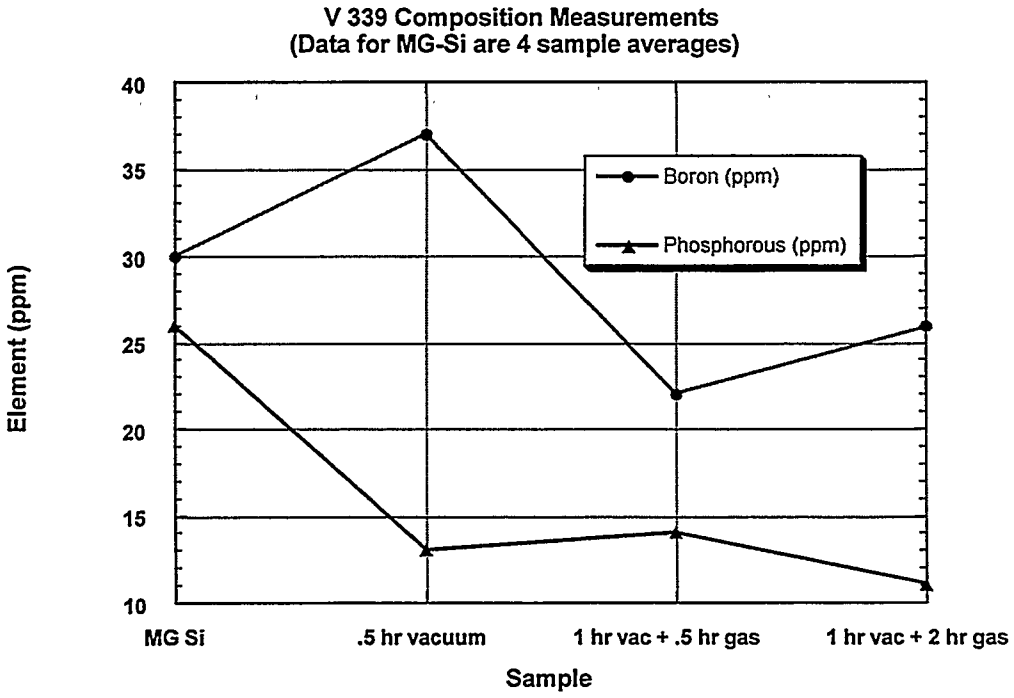

Figure 9. B and P compositions measured for Si melt V 339

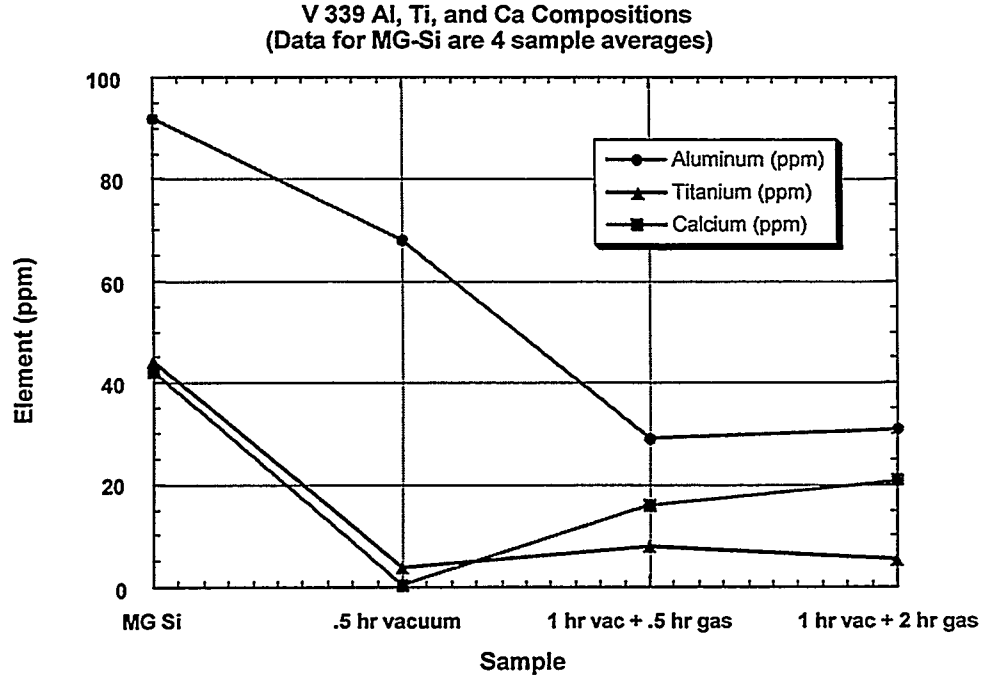

Figure 10. Al, Ti, and Ca compositions measured for Si melt V 339

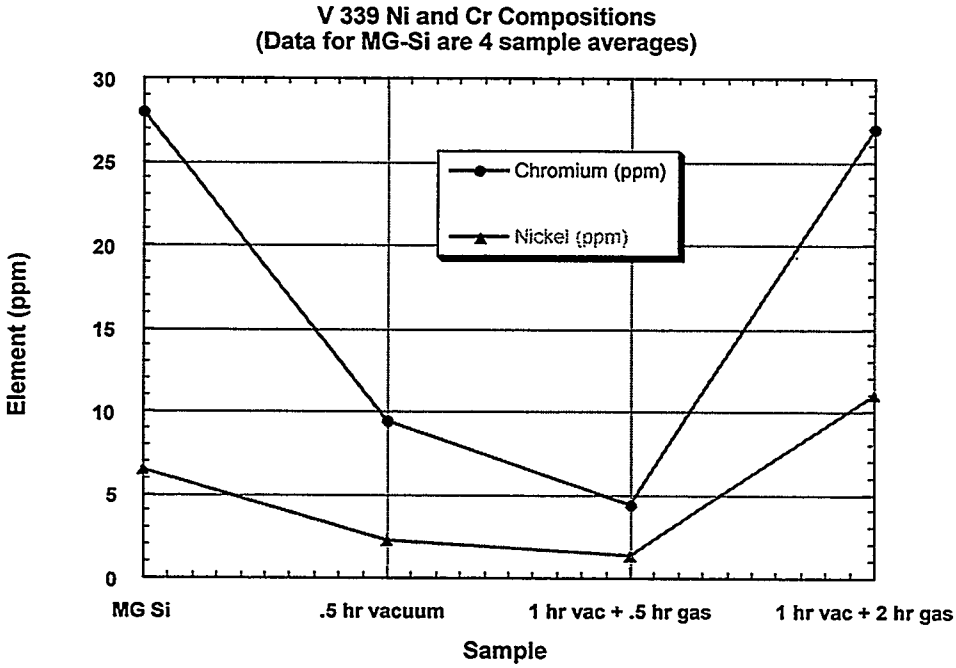

Figure 11. Cr and Ni compositions for Si melt V 339

C. Discussion and Conclusions

The results of these experiments show that exposure of molten MG Si to vacuum in the induction furnace did reduce levels of a number of impurity elements, including P and as well as several metallic species. Concentrations of these species were typically reduced by a factor of two or more after vacuum exposures of one-half to one hour. Measured vacuum levels during these high temperature vacuum exposures were typically 200-300 mtorr. It is likely that this gas pressure originated from outgassing of the crucible box with its packing sand, with water vapor was a major component. Dissociation of the water at the hot Si surface would have provided significant levels of hydrogen and oxygen for reaction with several of the species, as well as the Si. Prior to the melt V 339 experiment, the crucible box was baked out in vacuum at high temperature in an attempt to remove the moisture and any other volatiles; since the furnace pressures during vacuum treatment were not different between melts V 338 and V 339, this bakeout was incomplete.

Reduction of B levels either by vacuum treatment or by blowing with NH_3 were not achieved here. Thermodynamic models predict that the B dissolved in molten Si should react with active nitrogen from dissociated ammonia at the molten surface. The BN formed would be small clusters and would rapidly re-dissolve in the Si if they were not trapped. Possible trapping sites could be the crucible wall or a floating slag. The data suggest that the crucible walls were not effective trapping locations; this could be because the silica crucible was also reacting with the Si melt, and the surface was not stable. Additional work to develop a useful slag on molten Si would be necessary to further test the usefulness of blowing with ammonia gas.

Several engineering issues were identified during this work that would need to be addressed to optimize induction melting for Si processing.

1. Thermal transfer is poor from the graphite susceptor through the quartz crucible wall into the solid Si charge. Melt-in times of several hours are inefficient for this type of furnace. Since heat flow is from the outside in, it is important to avoid overheating the crucible, which can cause it to sag as well as chemically react with the Si. It is also thermally inefficient to use an induction furnace for many hours of reaction; runs of 10's of hours would be economically impractical.
2. The top of the molten Si ingot always freezes first due to radiative cooling. Since Si expands as it solidifies, subsurface molten Si exerts pressure and fractures the crucible. This results in loss of product as well as need for extensive cleanup and rebuilding of the crucible box and susceptor.
3. Reaction is continuous between the molten Si and the crucible and/or the furnace atmosphere. This generates large amounts of gaseous SiO which redeposit inside the furnace, particularly along the top rim of the crucible. This precludes tilt pouring the molten Si charge, since the Si reacts violently with the deposits.
4. Sampling the molten Si during the process remains a concern. The copper block dipper did obtain Si material, but it would be better to use a non-metallic sampler. Additional work is needed to develop a quartz tube sampling system.

III. Thermochemical Analysis for Al Removal from Polysilicon Melts

This section presents results from chemical equilibrium calculations that examine the likely effectiveness of various "gas blowing" treatments to remove impurities from polysilicon melts. The main body of this work is described in Sandia National Laboratories report number SAND99-1047 by P. Ho and J. M. Gee [5]. That report contains a description of the problem, calculational methods, and results for removal of C, B, P and Fe impurities. This supplement provides data and results for Al only, and is not meant to be a stand-alone document.

The calculational methods, input mixtures, and temperature/pressure conditions were the same as used previously, except for the addition of Al(cr) at the 0.001 level. Thermochemical data were obtained from several sources. The CHEMKIN thermodynamic database [6] contained data for Al, AlCl, $AlCl_2$, $AlCl_3$, Al_2Cl_6, AlH, AlH_2, AlH_3, Al_2H_6, AlMe, $AlMe_2$, H_2AlMe, HAlMe, $HAlMe_2$ (where Me denotes a methyl group) and Al(cr). Updated data for $AlMe_3$ and Al_2Me_6 were obtained from Harry Moffat's work on MOCVD precursors. The NASA thermochemical data base [7] provided information for $AlBO_2$, AlC, AlN, AlO, AlOCl, AlOH, AlO_2, AlO_2H, Al_2, Al_2O, Al_2O_2, HAlO, AlN(s), Al_2O_3(a), Al_2O_3(l), Al_2SiO_5(an) and $Al_6Si_2O_{13}$(s). Data for $AlCl_3$(s) and AlH_3(s) were taken from the Noring database [8], while data for Al_4C_3(cr) were obtained by fitting data from the JANAF Tables [9] to the appropriate polynomial form. Densities for the condensed phase species [Al(cr) = 2.702 g/cm^3, AlN(s) = 3.26, Al_2O_3(a) = 3.97, Al(l) = 2.39, $AlCl_3$(l) = 1.31] were obtained from the CRC [10], except for Al_2O_3(l) and AlH_3(s) where guesses were used. The list of Al-containing compounds is short enough that no effort to reduce the number of species was made, although many of the species were clearly not significant.

A. Results

The results of the equilibrium calculations are presented in two forms. Figures 12–22 give the distribution of Al among the gas, liquid, and solid phases as a function of temperature and pressure. Tables 5–15 list the corresponding dominant Al-containing chemical species in each phase, again as a function of temperature and pressure. As for the main study, the added gases investigated are: O_2, air, water vapor, wet air, HCl, Cl_2, Cl_2/O_2, $SiCl_4$, NH_3, NH_4OH and NH_4Cl.

The calculations included a small amount of Ar to avoid potential numerical problems in case all the gases react to form condensed products, making the volume too small.

The figures and tables show several trends:

1. As would be expected for a metal that melts at 660°C, there can be significant amounts of atomic Al in the gas, especially at higher temperatures and lower pressures. This suggests that Al might, to a limited extent, be removed by vaporization in the absence of added gases. Similar results were reported for P and Fe in the earlier study, although Al has smaller fractions in the vapor.
2. Most of the Al is generally present in the liquid phase, except when nitrogen is present in the system. In that case, AlN(s) dominates, especially at higher pressures and lower temperatures. Formation of AlN(s) should be kinetically limited, especially with N_2, but evaluating such considerations are beyond the scope of this study.
3. In the presence of chlorine, aluminum chlorides ($AlCl_2$ and Al_2Cl_6) can form in the gas, increasing the fraction of Al in the gas-phase somewhat above that from vaporization alone. However, formation of these chlorides is more significant at higher pressures, where there is less Al in the gas-phase, so this is probably not a major effect. However, at higher temperatures and pressure, substantial amounts of liquid $AlCl_3$ are predicted to be present at equilibrium, and this may be sufficiently less dense than liquid silicon to provide some separation possibilities.
4. For NH_3 and H_2O gas treatments, some AlH_2 formation is predicted. However, this is also favored at higher pressures where less of the Al is in the gas-phase, so this is probably not a very important effect.
5. In the presence of oxygen, significant amounts of liquid and solid Al_2O_3 can form, but may be difficult to separate from molten silicon. This is also favored at higher pressures and lower temperatures.

B. Discussion and Conclusions

The results of these equilibrium calculations can be qualitatively compared with silicon purification experiments in the literature. Khattak and Schmid [11] reported that they were able to reduce Al impurities in silicon by argon blowing (pressures of 0.2-0.3 Torr) or a combination of moist argon blowing and slagging. This is consistent with the results in Figures 14 and Table 7, indicating that some Al can be removed by evaporation, and that this removal is assisted by water vapor. Calculations done with Ar only (0.06) at 1650°C and 0.001 atm showed 15% of the Al in the vapor, as compared with 26% for water vapor (0.05 H_2O + 0.01 Ar) at the same conditions. (Note that a calculation done with 0.05 H_2 + 0.01Ar gave essentially the same results as pure argon at this high temperature and low pressure.) Dosaj et al., [12] and Hunt, et al. [13] reported that reactive gas blowing with Cl_2 or a Cl_2/O_2 mixture has been used to reduce the level of Al in silicon. This is consistent with the results presented in Figures. 17 and 18 and Tables 10 and 11, although the calculations suggest that, depending on the pressure and temperatures used, the observed reduction in Al might be due to evaporation as much as a chemical reaction. In contrast with these studies, Sakaguchi, et al. [14], addressed the reduction of Al impurities in the directional solidification part of their work, rather than in the gas blowing part of the study.

These chemical equilibrium calculations suggest that Al impurities are likely to be removed from molten silicon by gas-blowing techniques primarily via evaporation at relatively high temperatures and low pressures. This is similar to the results for P removal, with the caveat that Al will probably be harder to remove. In practice, the presence of the blowing gas, as opposed to simple evacuation, may be necessary to help "stir" the melt and transport gas-phase species out of the system. Alternatively, aluminum nitride, oxide, and/or condensed-phase chlorides should form in significant quantities under certain conditions. If they can be separated from the molten silicon, this could provide a different approach to Al impurity removal.

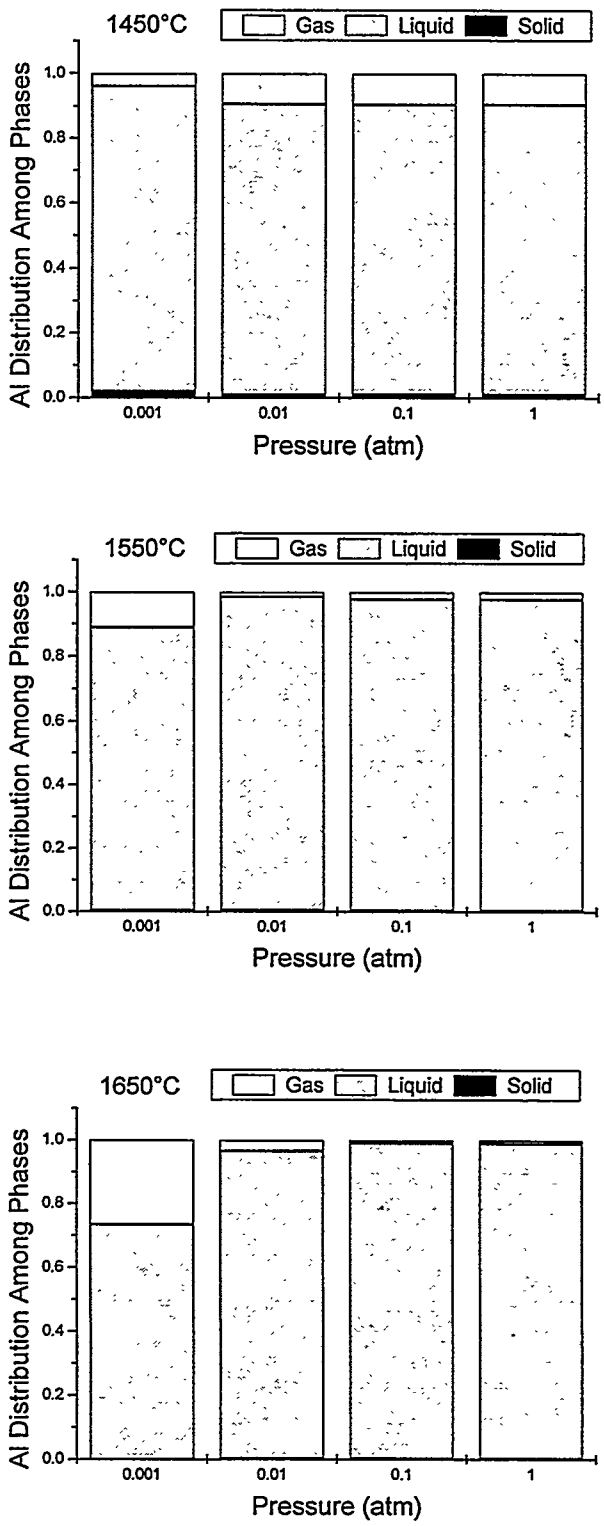

Figure 12. Distribution of aluminum among phases: $O_2 = 0.05$, Ar = 0.01.

Table 5: Dominant* chemical species for aluminum impurities in silicon with O_2/Ar addition.

Added Gases	Temperature (°C)	Pressure (atm)	Phase	Al-containing species
O_2 = 0.05 Ar = 0.01	1450	0.001	Gas Liquid Solid	Al Al(l) Al(cr), Al_2O_3(a)
O_2 = 0.05 Ar = 0.01	1450	0.01	Gas Liquid Solid	Al Al_2O_3(l), Al(l) Al(cr), Al_2O_3(a)
O_2 = 0.05 Ar = 0.01	1450	0.1 – 1.0	Gas Liquid Solid	Al Al_2O_3(l), Al(l) Al_2O_3(a), Al(cr)
O_2 = 0.05 Ar = 0.01	1550	0.001	Gas Liquid Solid	Al Al(l) Al(cr)
O_2 = 0.05 Ar = 0.01	1550	0.01	Gas Liquid Solid	Al Al(l), Al_2O_3(l) Al(cr), Al_2O_3(a)
O_2 = 0.05 Ar = 0.01	1550	0.1 – 1.0	Gas Liquid Solid	Al Al_2O_3(l), Al(l) Al_2O_3(a), Al(cr)
O_2 = 0.05 Ar = 0.01	1650	0.001	Gas Liquid Solid	Al Al(l) ---
O_2 = 0.05 Ar = 0.01	1650	0.01	Gas Liquid Solid	Al Al(l) Al(cr)
O_2 = 0.05 Ar = 0.01	1650	0.1 – 1.0	Gas Liquid Solid	Al Al(l), Al_2O_3(l) Al_2O_3(a), Al(cr)

* Chemical species are listed for each phase in order of decreasing mole fraction. If multiple species are listed, each represents at least ~10% of the aluminum in that phase.

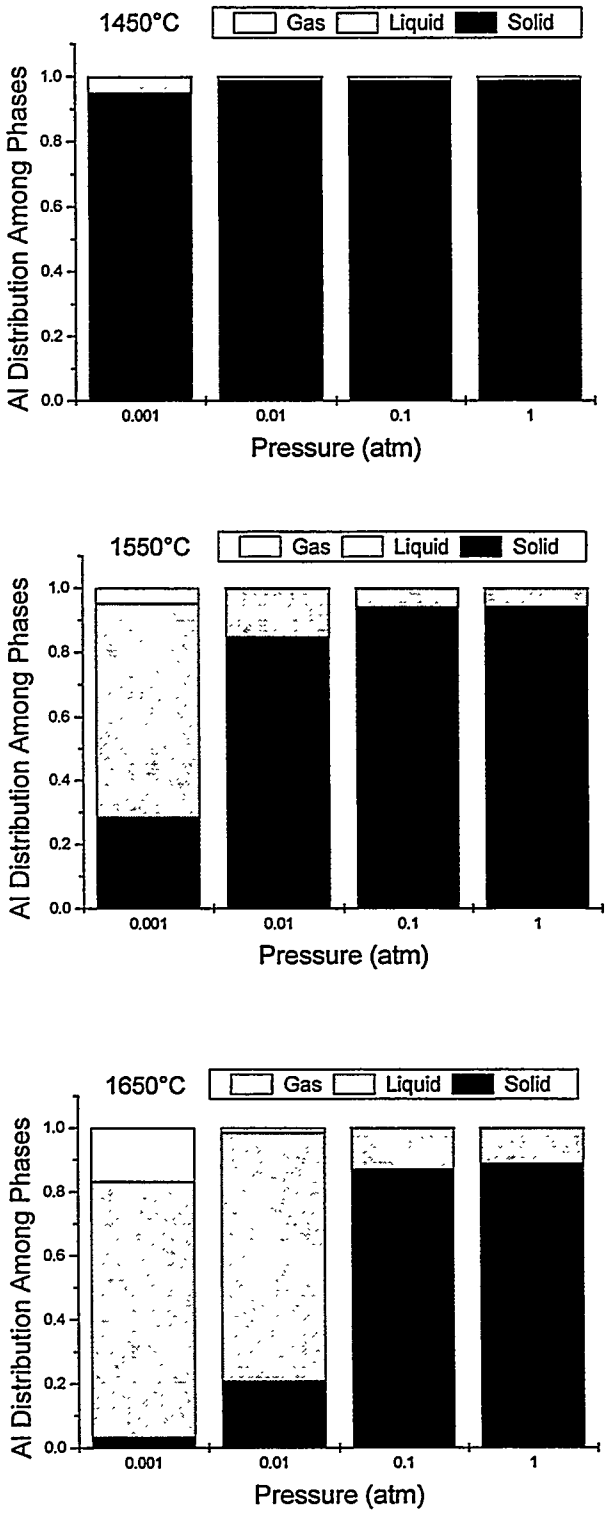

Figure 13. Distribution of aluminum among phases: $O_2 = 0.01$, $N_2 = 0.04$, Ar = 0.01.

Table 6. Dominant* chemical species for aluminum impurities in silicon with $O_2/N_2/Ar$ addition.

Added Gases	Temperature (°C)	Pressure (atm)	Phase	Al-containing species
$O_2 = 0.01$ $N_2 = 0.04$ $Ar = 0.01$	1450	0.001 – 1.0	Gas Liquid Solid	Al Al(l) AlN(s)
$O_2 = 0.01$ $N_2 = 0.04$ $Ar = 0.01$	1550	0.001 – 1.0	Gas Liquid Solid	Al Al(l) AlN(s)
$O_2 = 0.01$ $N_2 = 0.04$ $Ar = 0.01$	1650	0.001 – 1.0	Gas Liquid Solid	Al Al(l) AlN(s)

* Chemical species are listed for each phase in order of decreasing mole fraction. If multiple species are listed, each represents at least ~10% of the aluminum in that phase.

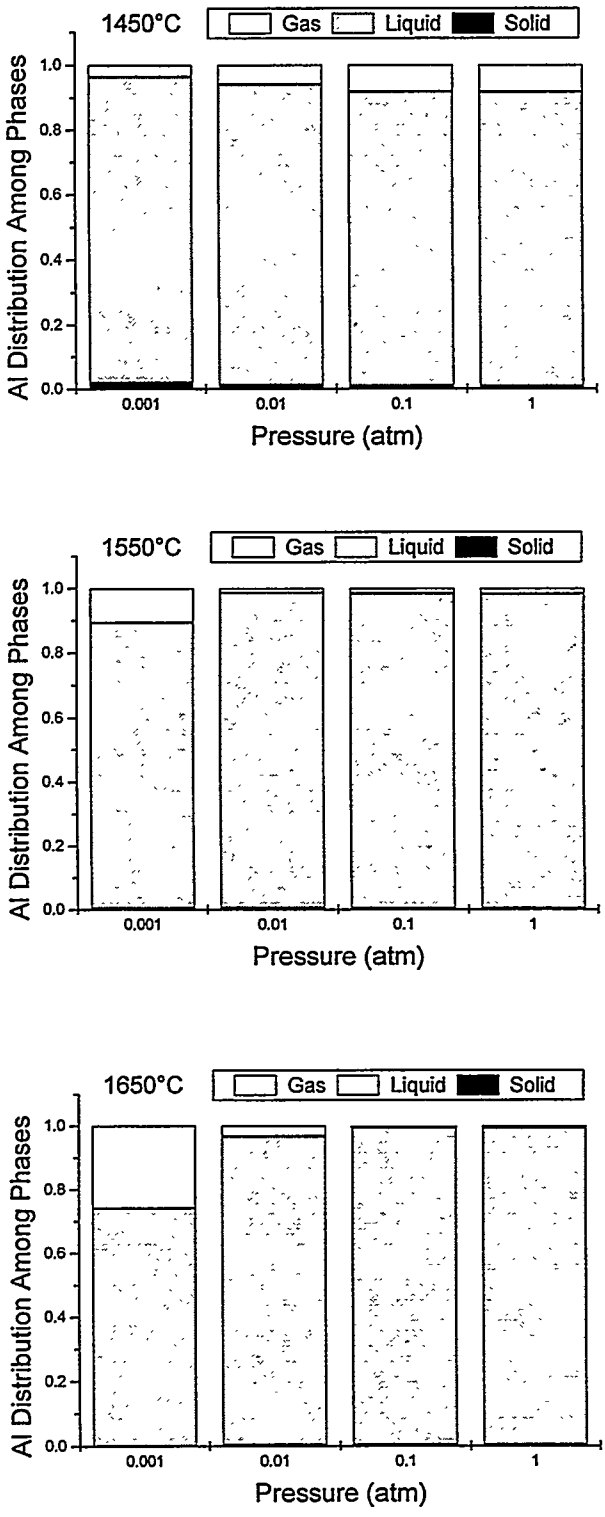

Figure 14. Distribution of aluminum among phases: $H_2O = 0.05$, Ar = 0.01.

Table 7. Dominant* chemical species for aluminum impurities in silicon with H_2O/Ar addition.

Added Gases	Temperature (°C)	Pressure (atm)	Phase	Al-containing species
H_2O = 0.05 Ar = 0.01	1450	0.001	Gas Liquid Solid	Al Al(l) Al(cr)
H_2O = 0.05 Ar = 0.01	1450	0.01	Gas Liquid Solid	Al, AlH_2 Al(l), Al_2O_3(l) Al_2O_3(a), Al(cr)
H_2O = 0.05 Ar = 0.01	1450	0.1 – 1.0	Gas Liquid Solid	AlH_2, Al Al(l), Al_2O_3(l) Al_2O_3(a), Al(cr)
H_2O = 0.05 Ar = 0.01	1550	0.001	Gas Liquid Solid	Al Al(l) Al(cr)
H_2O = 0.05 Ar = 0.01	1550	0.01	Gas Liquid Solid	Al Al(l) Al(cr), Al_2O_3(a)
H_2O = 0.05 Ar = 0.01	1550	0.1	Gas Liquid Solid	Al, AlH_2 Al(l), Al_2O_3(l) Al_2O_3(a), Al(cr)
H_2O = 0.05 Ar = 0.01	1550	1.0	Gas Liquid Solid	AlH_2, Al Al(l), Al_2O_3(l) Al_2O_3(a), Al(cr)
H_2O = 0.05 Ar = 0.01	1650	0.001	Gas Liquid Solid	Al Al(l) ---
H_2O = 0.05 Ar = 0.01	1650	0.01	Gas Liquid Solid	Al Al(l) Al(cr)
H_2O = 0.05 Ar = 0.01	1650	0.1	Gas Liquid Solid	Al, AlH_2 Al(l), Al_2O_3(l) Al(cr), Al_2O_3(a)
H_2O = 0.05 Ar = 0.01	1650	1.0	Gas Liquid Solid	AlH_2, Al Al(l), Al_2O_3(l) Al_2O_3(a), Al(cr)

* Chemical species are listed for each phase in order of decreasing mole fraction. If multiple species are listed, each represents at least ~10% of the aluminum in that phase.

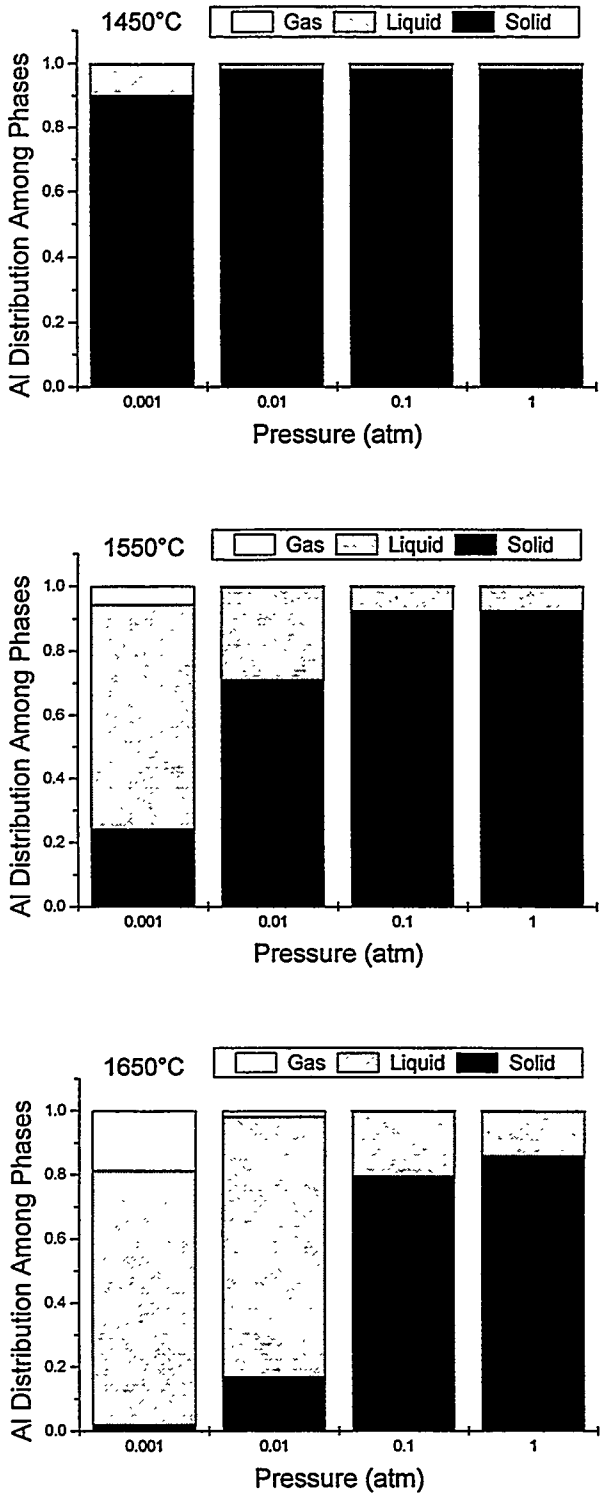

Figure 15. Distribution of aluminum among phases: $H_2O = 0.01$, $O_2 = 0.008$, $N_2 = 0.032$, Ar = 0.01.

Table 8. Dominant* chemical species for aluminum impurities in silicon with $H_2O/O_2/N_2/Ar$ addition.

Added Gases	Temperature (°C)	Pressure (atm)	Phase	Al-containing species
$H_2O = 0.01$ $O_2 = 0.008$ $N_2 = 0.032$ $Ar = 0.01$	1450	0.001 – 0.01	Gas Liquid Solid	Al Al(l) AlN(s)
$H_2O = 0.01$ $O_2 = 0.008$ $N_2 = 0.032$ $Ar = 0.01$	1450	0.1	Gas Liquid Solid	Al, AlH_2 Al(l) AlN(s)
$H_2O = 0.01$ $O_2 = 0.008$ $N_2 = 0.032$ $Ar = 0.01$	1450	1.0	Gas Liquid Solid	AlH_2, Al Al(l) AlN(s)
$H_2O = 0.01$ $O_2 = 0.008$ $N_2 = 0.032$ $Ar = 0.01$	1550	0.001 – 0.01	Gas Liquid Solid	Al Al(l) AlN(s)
$H_2O = 0.01$ $O_2 = 0.008$ $N_2 = 0.032$ $Ar = 0.01$	1550	0.1	Gas Liquid Solid	Al, AlH_2 Al(l) AlN(s)
$H_2O = 0.01$ $O_2 = 0.008$ $N_2 = 0.032$ $Ar = 0.01$	1550	1.0	Gas Liquid Solid	AlH_2, Al Al(l) AlN(s)
$H_2O = 0.01$ $O_2 = 0.008$ $N_2 = 0.032$ $Ar = 0.01$	1650	0.001 – 0.01	Gas Liquid Solid	Al Al(l) AlN(s)
$H_2O = 0.01$ $O_2 = 0.008$ $N_2 = 0.032$ $Ar = 0.01$	1650	0.1	Gas Liquid Solid	Al, AlH_2 Al(l) AlN(s)
$H_2O = 0.01$ $O_2 = 0.008$ $N_2 = 0.032$ $Ar = 0.01$	1650	1.0	Gas Liquid Solid	AlH_2, Al Al(l) AlN(s)

* Chemical species are listed for each phase in order of decreasing mole fraction. If multiple species are listed, each represents at least ~10% of the aluminum in that phase.

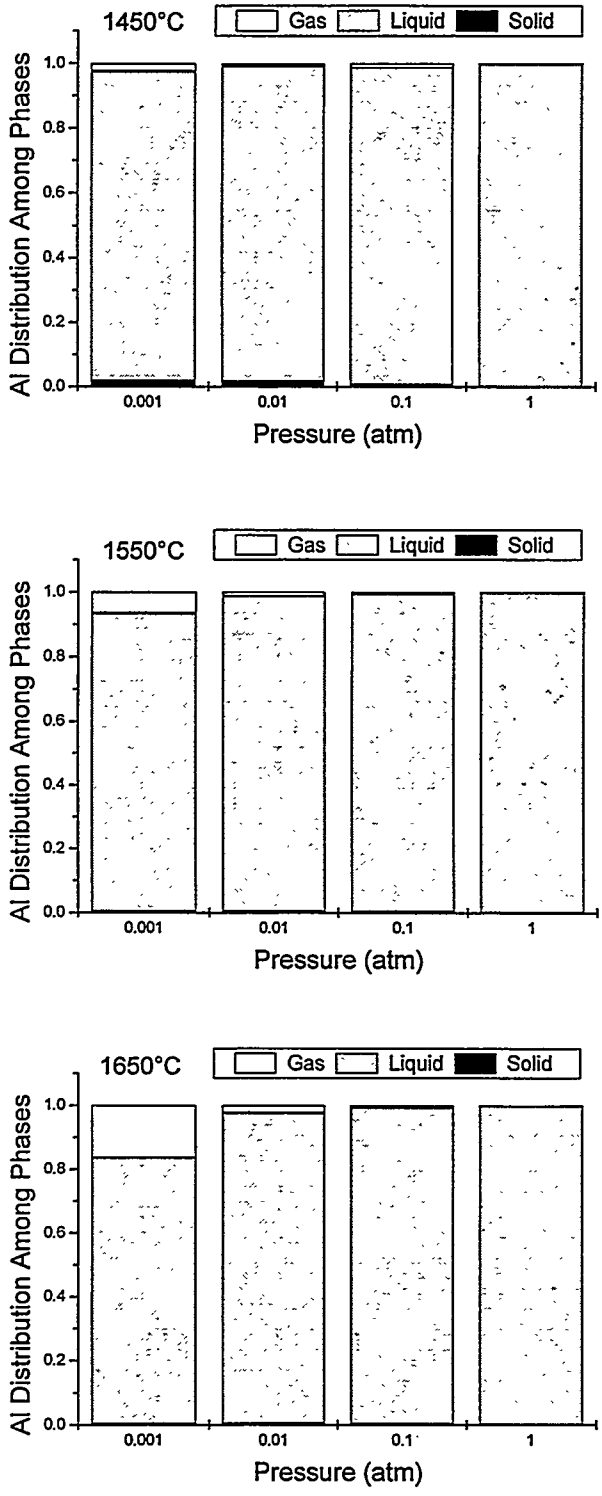

Figure 16. Distribution of aluminum among phases: HCl = 0.05, Ar = 0.01.

Table 9. Dominant* chemical species for aluminum impurities in silicon with HCl/Ar addition.

Added Gases	Temperature (°C)	Pressure (atm)	Phase	Al-containing species
HCl = 0.05 Ar = 0.01	1450	0.001	Gas Liquid Solid	Al, $AlCl_2$ Al(l) Al(cr)
HCl = 0.05 Ar = 0.01	1450	0.01	Gas Liquid Solid	$AlCl_2$, Al, Al_2Cl_6 Al(l) Al(cr)
HCl = 0.05 Ar = 0.01	1450	0.1	Gas Liquid Solid	Al_2Cl_6, $AlCl_2$ $AlCl_3$(l), Al(l) Al(cr)
HCl = 0.05 Ar = 0.01	1450	1.0	Gas Liquid Solid	Al_2Cl_6, $AlCl_2$ $AlCl_3$(l) Al(cr)
HCl = 0.05 Ar = 0.01	1550	0.001 – 0.01	Gas Liquid Solid	Al, $AlCl_2$ Al(l) Al(cr)
HCl = 0.05 Ar = 0.01	1550	0.1	Gas Liquid Solid	$AlCl_2$, Al_2Cl_6 Al(l), $AlCl_3$(l) Al(cr)
HCl = 0.05 Ar = 0.01	1550	1.0	Gas Liquid Solid	Al_2Cl_6, $AlCl_2$ $AlCl_3$(l), Al(l) Al(cr)
HCl = 0.05 Ar = 0.01	1650	0.001	Gas Liquid Solid	Al Al(l) Al(cr)
HCl = 0.05 Ar = 0.01	1650	0.01	Gas Liquid Solid	Al, $AlCl_2$ Al(l) Al(cr)
HCl = 0.05 Ar = 0.01	1650	0.1	Gas Liquid Solid	$AlCl_2$, Al_2Cl_6 Al(l), $AlCl_3$(l) Al(cr)
HCl = 0.05 Ar = 0.01	1650	1.0	Gas Liquid Solid	$AlCl_2$, Al $AlCl_3$(l), Al(l) Al(cr)

* Chemical species are listed for each phase in order of decreasing mole fraction. If multiple species are listed, each represents at least ~10% of the aluminum in that phase.

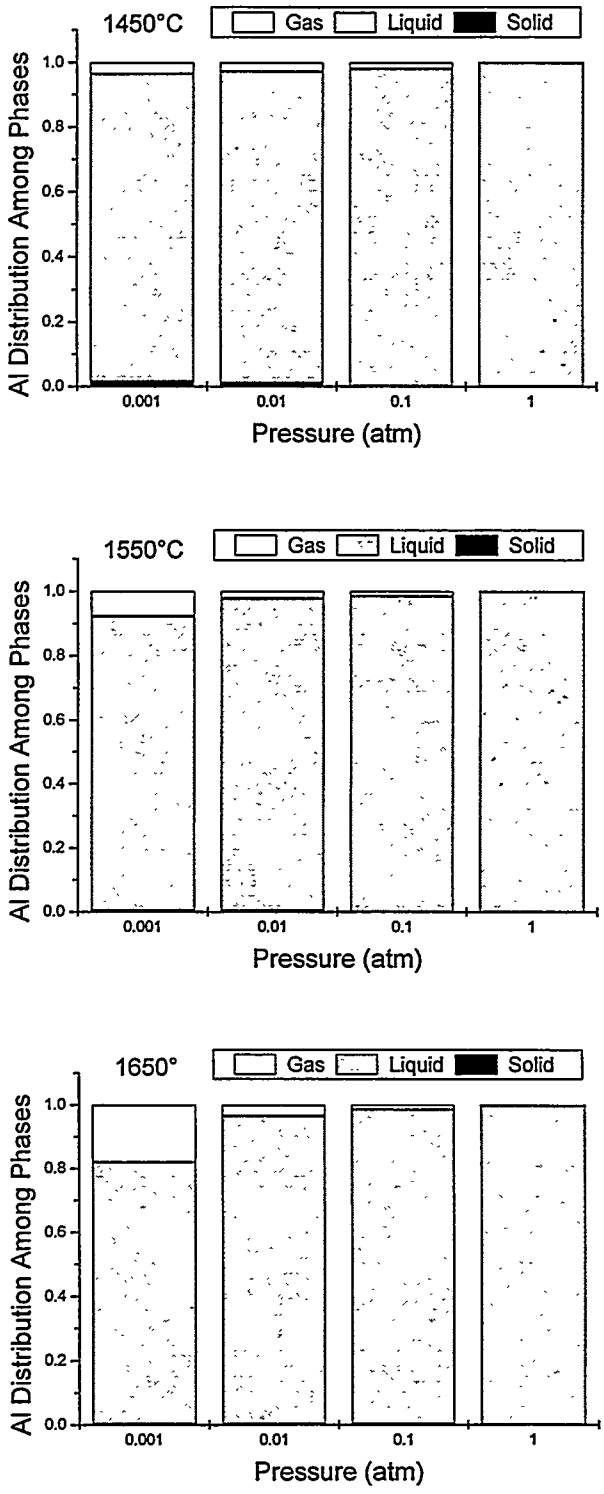

Figure 17. Distribution of aluminum among phases: $Cl_2 = 0.05$, Ar = 0.01.

Table 10. Dominant* chemical species for aluminum impurities in silicon with Cl_2/Ar addition.

Added Gases	Temperature (°C)	Pressure (atm)	Phase	Al-containing species
Cl_2 = 0.05 Ar = 0.01	1450	0.001	Gas Liquid Solid	Al, $AlCl_2$ Al(l) Al(cr)
Cl_2 = 0.05 Ar = 0.01	1450	0.01	Gas Liquid Solid	$AlCl_2$, Al_2Cl_6 Al(l), $AlCl_3$(l) Al(cr)
Cl_2 = 0.05 Ar = 0.01	1450	0.1	Gas Liquid Solid	Al_2Cl_6, $AlCl_2$ $AlCl_3$(l), Al(l) Al(cr)
Cl_2 = 0.05 Ar = 0.01	1450	1.0	Gas Liquid Solid	Al_2Cl_6 $AlCl_3$(l) Al(cr), $AlCl_3$(s)
Cl_2 = 0.05 Ar = 0.01	1550	0.001	Gas Liquid Solid	Al, $AlCl_2$ Al(l) Al(cr)
Cl_2 = 0.05 Ar = 0.01	1550	0.01	Gas Liquid Solid	$AlCl_2$, Al Al(l), $AlCl_3$(l) Al(cr)
Cl_2 = 0.05 Ar = 0.01	1550	0.1	Gas Liquid Solid	Al_2Cl_6, $AlCl_2$ $AlCl_3$(l), Al(l) Al(cr)
Cl_2 = 0.05 Ar = 0.01	1550	1.0	Gas Liquid Solid	Al_2Cl_6, $AlCl_2$ $AlCl_3$(l) Al(cr), $AlCl_3$(s)
Cl_2 = 0.05 Ar = 0.01	1650	0.001	Gas Liquid Solid	Al, $AlCl_2$ Al(l) Al(cr)
Cl_2 = 0.05 Ar = 0.01	1650	0.01	Gas Liquid Solid	Al, $AlCl_2$ Al(l) Al(cr)
Cl_2 = 0.05 Ar = 0.01	1650	0.1	Gas Liquid Solid	$AlCl_2$, Al_2Cl_6 $AlCl_3$(l), Al(l) Al(cr)
Cl_2 = 0.05 Ar = 0.01	1650	1.0	Gas Liquid Solid	Al_2Cl_6, $AlCl_2$ $AlCl_3$(l) Al(cr)

* Chemical species are listed for each phase in order of decreasing mole fraction. If multiple species are listed, each represents at least ~10% of the aluminum in that phase.

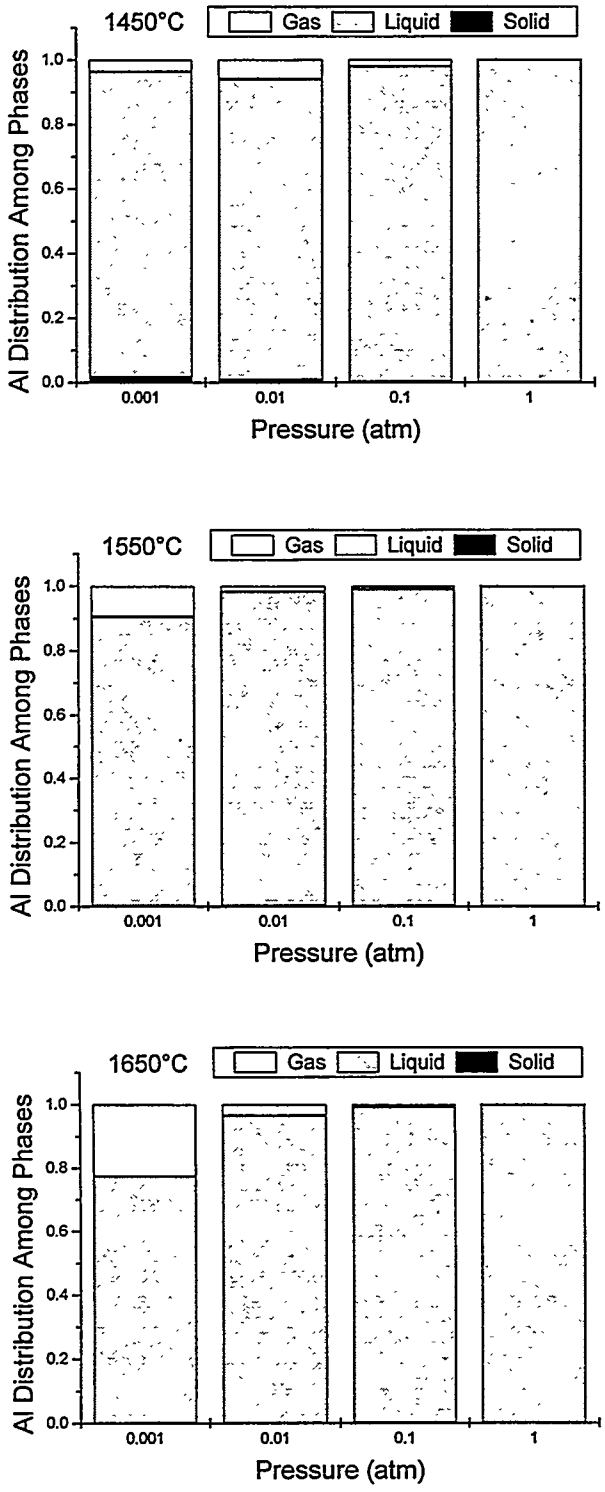

Figure 18. Distribution of aluminum among phases: $Cl_2 = 0.025$, $O_2 = 0.025$, Ar = 0.01.

Table 11. Dominant* chemical species for aluminum impurities in silicon with Cl_2/O_2/Ar addition.

Added Gases	Temperature (°C)	Pressure (atm)	Phase	Al-containing species
Cl_2 = 0.025 O_2 = 0.025 Ar = 0.01	1450	0.001	Gas Liquid Solid	Al, $AlCl_2$ Al(l) Al(cr)
Cl_2 = 0.025 O_2 = 0.025 Ar = 0.01	1450	0.01	Gas Liquid Solid	$AlCl_2$, Al, Al_2Cl_6 Al(l), Al_2O_3(l) Al_2O_3(a), Al(cr)
Cl_2 = 0.025 O_2 = 0.025 Ar = 0.01	1450	0.1	Gas Liquid Solid	Al_2Cl_6, $AlCl_2$ $AlCl_3$(l), Al(l) Al_2O_3(a), Al(cr)
Cl_2 = 0.025 O_2 = 0.025 Ar = 0.01	1450	1.0	Gas Liquid Solid	Al_2Cl_6 $AlCl_3$(l) Al(cr), Al_2O_3(a)
Cl_2 = 0.025 O_2 = 0.025 Ar = 0.01	1550	0.001	Gas Liquid Solid	Al, $AlCl_2$ Al(l) Al(cr)
Cl_2 = 0.025 O_2 = 0.025 Ar = 0.01	1550	0.01	Gas Liquid Solid	Al, $AlCl_2$ Al(l) Al(cr), Al_2O_3(a)
Cl_2 = 0.025 O_2 = 0.025 Ar = 0.01	1550	0.1	Gas Liquid Solid	$AlCl_2$, Al_2Cl_6, $AlCl_3$(l), Al(l), Al_2O_3(l) Al_2O_3(a), Al(cr)
Cl_2 = 0.025 O_2 = 0.025 Ar = 0.01	1550	1.0	Gas Liquid Solid	Al_2Cl_6, $AlCl_2$ $AlCl_3$(l), Al(l) Al(cr), Al_2O_3(a)
Cl_2 = 0.025 O_2 = 0.025 Ar = 0.01	1650	0.001	Gas Liquid Solid	Al Al(l) ---
Cl_2 = 0.025 O_2 = 0.025 Ar = 0.01	1650	0.01	Gas Liquid Solid	Al, $AlCl_2$ Al(l) ---
Cl_2 = 0.025 O_2 = 0.025 Ar = 0.01	1650	0.1	Gas Liquid Solid	$AlCl_2$, Al, Al_2Cl_6 Al(l), $AlCl_3$(l), Al_2O_3(l) Al(cr), Al_2O_3(a)
Cl_2 = 0.025 O_2 = 0.025 Ar = 0.01	1650	1.0	Gas Liquid Solid	Al_2Cl_6, $AlCl_2$ $AlCl_3$(l) Al(cr), Al_2O_3(a)

* Chemical species are listed for each phase in order of decreasing mole fraction. If multiple species are listed, each represents at least ~10% of the aluminum in that phase.

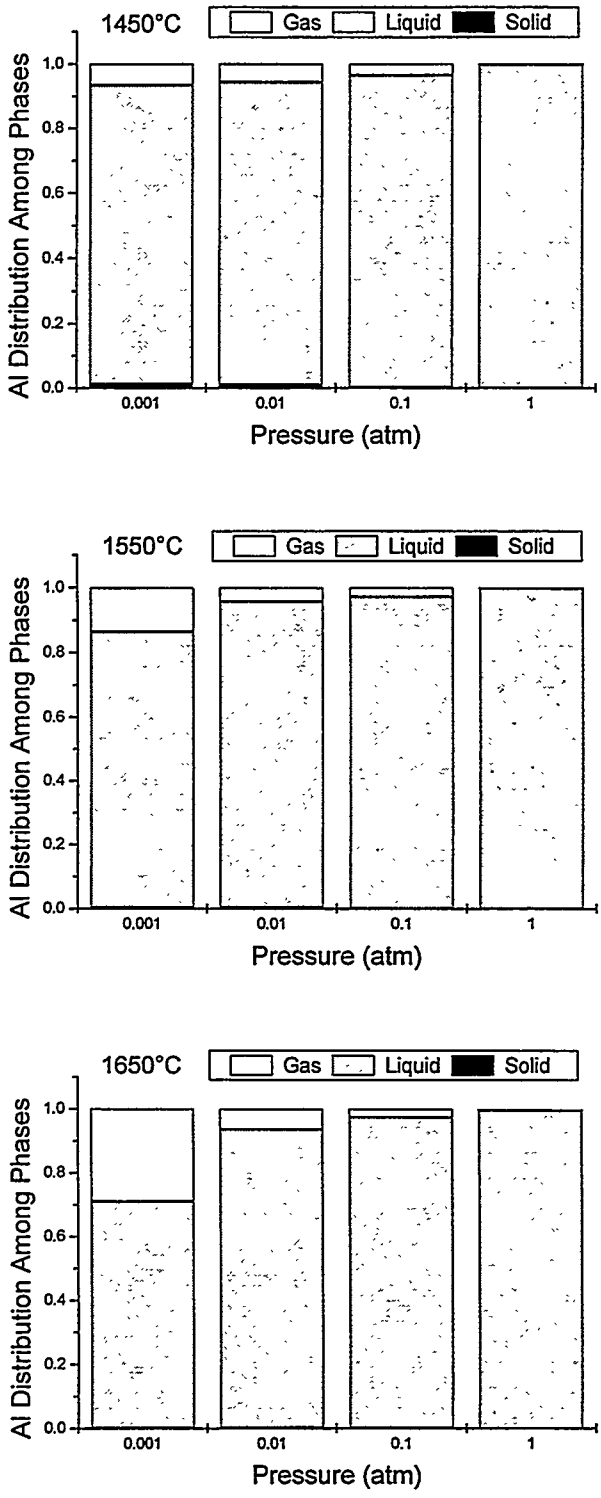

Figure 19. Distribution of aluminum among phases: $SiCl_4 = 0.05$, Ar = 0.01.

Table 12. Dominant* chemical species for aluminum impurities in silicon with $SiCl_4$/Ar addition.

Added Gases	Temperature (°C)	Pressure (atm)	Phase	Al-containing species
$SiCl_4$ = 0.05 Ar = 0.01	1450	0.001	Gas Liquid Solid	Al, $AlCl_2$ Al(l) Al(cr)
$SiCl_4$ = 0.05 Ar = 0.01	1450	0.01	Gas Liquid Solid	$AlCl_2$, Al_2Cl_6 Al(l), $AlCl_3$(l) Al(cr)
$SiCl_4$ = 0.05 Ar = 0.01	1450	0.1	Gas Liquid Solid	Al_2Cl_6, $AlCl_2$ $AlCl_3$(l), Al(l) Al(cr)
$SiCl_4$ = 0.05 Ar = 0.01	1450	1.0	Gas Liquid Solid	Al_2Cl_6 $AlCl_3$(l) Al(cr), $AlCl_3$(s)
$SiCl_4$ = 0.05 Ar = 0.01	1550	0.001	Gas Liquid Solid	Al, $AlCl_2$ Al(l) Al(cr)
$SiCl_4$ = 0.05 Ar = 0.01	1550	0.01	Gas Liquid Solid	$AlCl_2$, Al Al(l), $AlCl_3$(l) Al(cr)
$SiCl_4$ = 0.05 Ar = 0.01	1550	0.1	Gas Liquid Solid	Al_2Cl_6, $AlCl_2$ $AlCl_3$(l), Al(l) Al(cr)
$SiCl_4$ = 0.05 Ar = 0.01	1550	1.0	Gas Liquid Solid	Al_2Cl_6, $AlCl_2$ $AlCl_3$(l) Al(cr), $AlCl_3$(s)
$SiCl_4$ = 0.05 Ar = 0.01	1650	0.001	Gas Liquid Solid	Al, $AlCl_2$ Al(l) Al(cr)
$SiCl_4$ = 0.05 Ar = 0.01	1650	0.01	Gas Liquid Solid	$AlCl_2$, Al Al(l) Al(cr)
$SiCl_4$ = 0.05 Ar = 0.01	1650	0.1	Gas Liquid Solid	$AlCl_2$, Al_2Cl_6 $AlCl_3$(l), Al(l) Al(cr)
$SiCl_4$ = 0.05 Ar = 0.01	1650	1.0	Gas Liquid Solid	Al_2Cl_6, $AlCl_2$ $AlCl_3$(l) Al(cr)

* Chemical species are listed for each phase in order of decreasing mole fraction. If multiple species are listed, each represents at least ~10% of the aluminum in that phase.

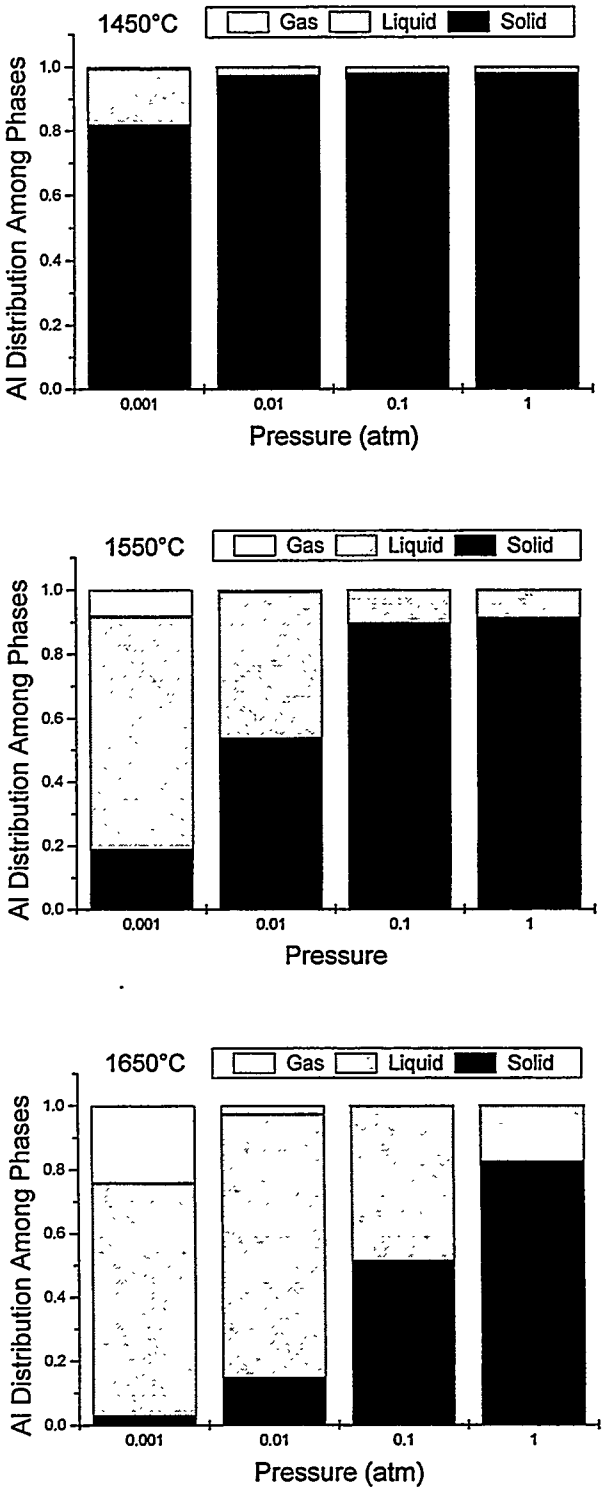

Figure 20. Distribution of aluminum among phases: $NH_3 = 0.05$, Ar = 0.01.

Table 13. Dominant* chemical species for aluminum impurities in silicon with NH_3/Ar addition.

Added Gases	Temperature (°C)	Pressure (atm)	Phase	Al-containing species
NH_3 = 0.05 Ar = 0.01	1450	0.001	Gas Liquid Solid	Al Al(l) AlN(s)
NH_3 = 0.05 Ar = 0.01	1450	0.01	Gas Liquid Solid	Al, AlH_2 Al(l) AlN(s)
NH_3 = 0.05 Ar = 0.01	1450	0.1	Gas Liquid Solid	AlH_2, Al Al(l) AlN(s)
NH_3 = 0.05 Ar = 0.01	1450	1.0	Gas Liquid Solid	AlH_2 Al(l) AlN(s)
NH_3 = 0.05 Ar = 0.01	1550	0.001 – 0.01	Gas Liquid Solid	Al Al(l) AlN(s)
NH_3 = 0.05 Ar = 0.01	1550	0.1	Gas Liquid Solid	Al, AlH_2 Al(l) AlN(s)
NH_3 = 0.05 Ar = 0.01	1550	1.0	Gas Liquid Solid	AlH_2, Al Al(l) AlN(s)
NH_3 = 0.05 Ar = 0.01	1650	0.001	Gas Liquid Solid	Al Al(l) AlN(s), Al(cr)
NH_3 = 0.05 Ar = 0.01	1650	0.01	Gas Liquid Solid	Al Al(l) AlN(s)
NH_3 = 0.05 Ar = 0.01	1650	0.1	Gas Liquid Solid	Al, AlH_2 Al(l) AlN(s)
NH_3 = 0.05 Ar = 0.01	1650	1.0	Gas Liquid Solid	AlH_2, Al Al(l) AlN(s)

* Chemical species are listed for each phase in order of decreasing mole fraction. If multiple species are listed, each represents at least ~10% of the aluminum in that phase.

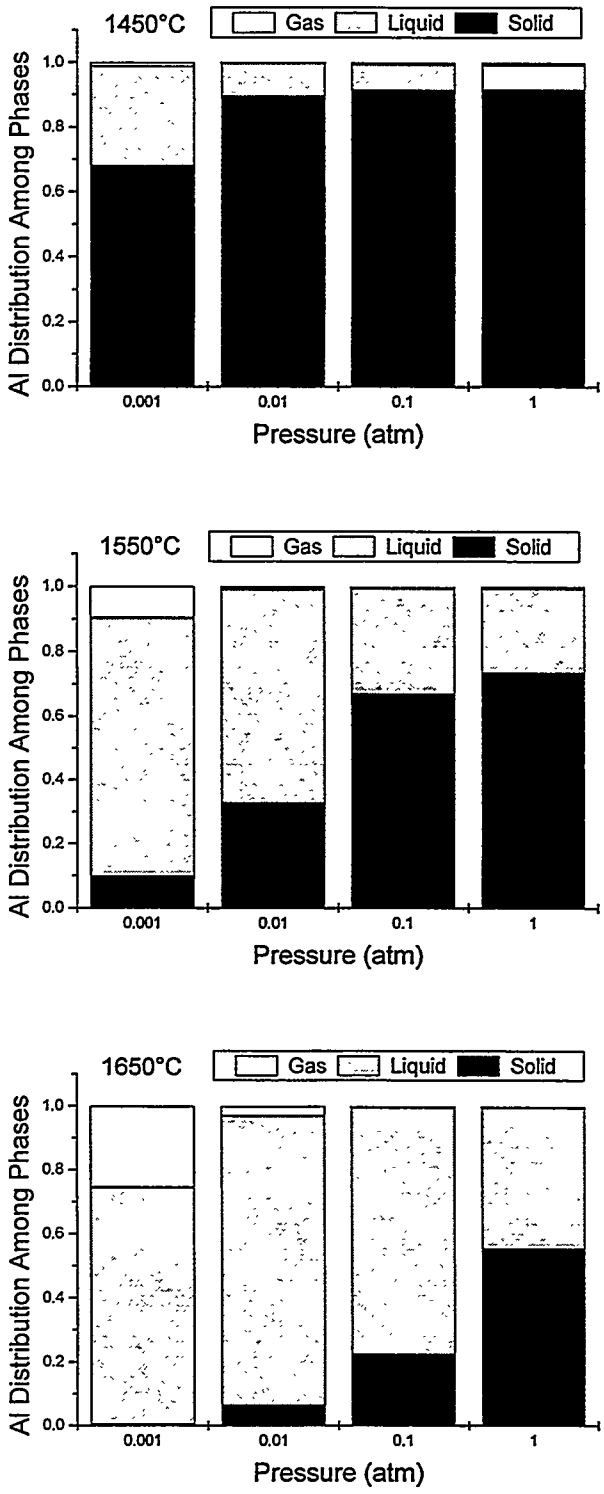

Figure 21. Distribution of aluminum among phases: $NH_3 = 0.015$, $H_2O = 0.035$, Ar = 0.01.

Table 14. Dominant* chemical species for aluminum impurities in silicon with NH_3/H_2O/Ar addition.

Added Gases	Temperature (°C)	Pressure (atm)	Phase	Al-containing species
NH_3 = 0.015 H_2O = 0.035 Ar = 0.01	1450	0.001 – 0.01	Gas Liquid Solid	Al Al(l) AlN(s)
NH_3 = 0.015 H_2O = 0.035 Ar = 0.01	1450	0.1 – 1.0	Gas Liquid Solid	AlH_2, Al Al(l), Al_2O_3(l) AlN(s)
NH_3 = 0.015 H_2O = 0.035 Ar = 0.01	1550	0.001 – 0.01	Gas Liquid Solid	Al Al(l) AlN(s)
NH_3 = 0.015 H_2O = 0.035 Ar = 0.01	1550	0.1	Gas Liquid Solid	Al, AlH_2 Al(l), Al_2O_3(l) AlN(s)
NH_3 = 0.015 H_2O = 0.035 Ar = 0.01	1550	1.0	Gas Liquid Solid	AlH_2, Al Al(l), Al_2O_3(l) AlN(s)
NH_3 = 0.015 H_2O = 0.035 Ar = 0.01	1650	0.001	Gas Liquid Solid	Al Al(l) AlN(s), Al(cr)
NH_3 = 0.015 H_2O = 0.035 Ar = 0.01	1650	0.01	Gas Liquid Solid	Al Al(l) AlN(s)
NH_3 = 0.015 H_2O = 0.035 Ar = 0.01	1650	0.1	Gas Liquid Solid	Al, AlH_2 Al(l) AlN(s)
NH_3 = 0.015 H_2O = 0.035 Ar = 0.01	1650	1.0	Gas Liquid Solid	AlH_2, Al Al(l), Al_2O_3(l) AlN(s)

* Chemical species are listed for each phase in order of decreasing mole fraction. If multiple species are listed, each represents at least ~10% of the aluminum in that phase.

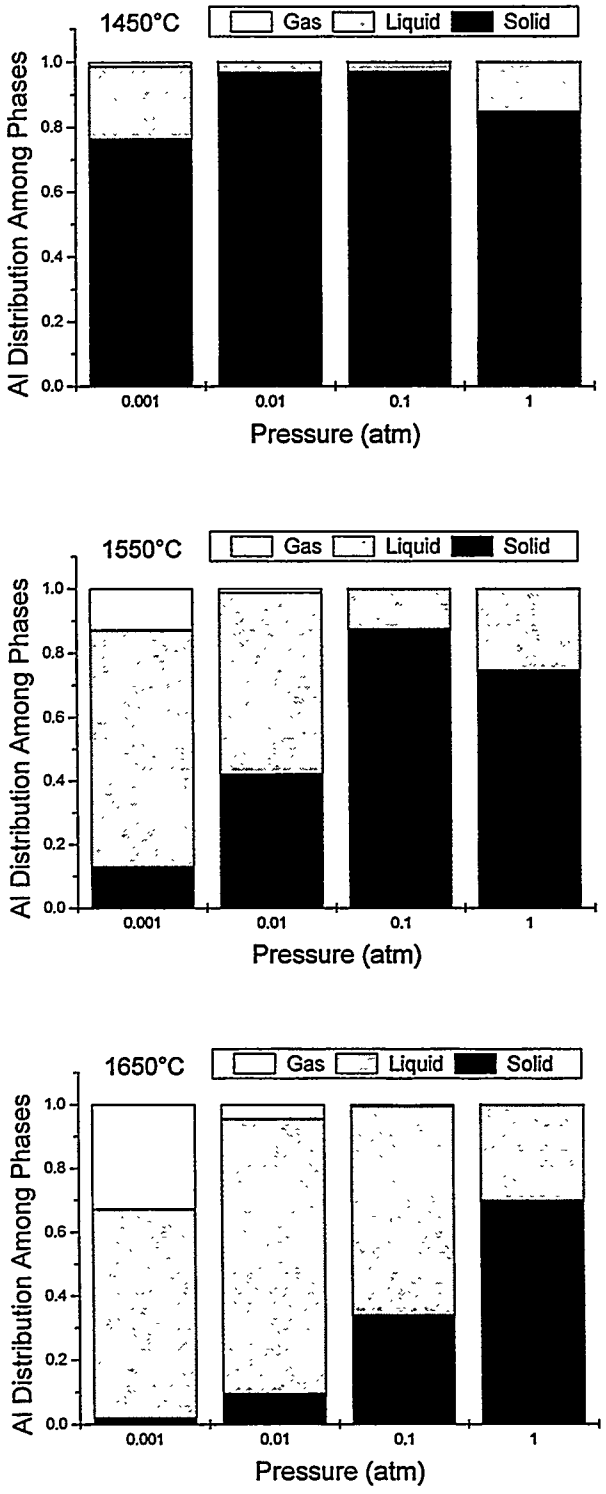

Figure 22. Distribution of aluminum among phases: $NH_4Cl = 0.05$, Ar = 0.01.

Table 15. Dominant* chemical species for aluminum impurities in silicon with NH_4Cl/Ar addition.

Added Gases	Temperature (°C)	Pressure (atm)	Phase	Al-containing species
NH_4Cl = 0.05 Ar = 0.01	1450	0.001	Gas Liquid Solid	Al Al(l) AlN(s)
NH_4Cl = 0.05 Ar = 0.01	1450	0.01	Gas Liquid Solid	Al, $AlCl_2$ Al(l) AlN(s)
NH_4Cl = 0.05 Ar = 0.01	1450	0.1	Gas Liquid Solid	$AlCl_2$, Al, AlH_2 Al(l), $AlCl_3$(l) AlN(s)
NH_4Cl = 0.05 Ar = 0.01	1450	1.0	Gas Liquid Solid	Al_2Cl_6, $AlCl_2$ $AlCl_3$(l), Al(l) AlN(s)
NH_4Cl = 0.05 Ar = 0.01	1550	0.001	Gas Liquid Solid	Al Al(l) AlN(s)
NH_4Cl = 0.05 Ar = 0.01	1550	0.01	Gas Liquid Solid	Al, $AlCl_2$ Al(l) AlN(s)
NH_4Cl = 0.05 Ar = 0.01	1550	0.1	Gas Liquid Solid	$AlCl_2$, Al, AlH_2 Al(l), $AlCl_3$(l) AlN(s)
NH_4Cl = 0.05 Ar = 0.01	1550	1.0	Gas Liquid Solid	$AlCl_2$, Al_2Cl_6, AlH_2 $AlCl_3$(l), Al(l) AlN(s)
NH_4Cl = 0.05 Ar = 0.01	1650	0.001	Gas Liquid Solid	Al Al(l) AlN(s), Al(cr)
NH_4Cl = 0.05 Ar = 0.01	1650	0.01	Gas Liquid Solid	Al Al(l) AlN(s)
NH_4Cl = 0.05 Ar = 0.01	1650	0.1	Gas Liquid Solid	Al, $AlCl_2$, AlH_2 Al(l) AlN(s)
NH_4Cl = 0.05 Ar = 0.01	1650	1.0	Gas Liquid Solid	$AlCl_2$, AlH_2, Al, Al_2Cl_6 Al(l), $AlCl_3$(l) AlN(s)

* Chemical species are listed for each phase in order of decreasing mole fraction. If multiple species are listed, each represents at least ~10% of the aluminum in that phase.

References

1. G. Lutwack, **Flat-Plate Solar Array Project Final Report: Volume II – Silicon Material,** JPL publication 86-31 (1986).
2. V.D. Dosaj, L.P. Hunt, and L.D. Crossman, Single crystal silicon ingot pulled from chemically-upgraded metallurgical-grade silicon, **11th IEEE Photo. Spec. Conf.**, 275-279 (1975).
3. L.P. Hunt, *et al.*, Production of solar-grade silicon from purified metallurgical silicon, **12th IEEE Photo. Spec. Conf.**, 125-129 (1977).
4. Y. Sakaguchi, *et al.*, Purification of metallic grade silicon up to solar grade by NEDO melt purification process, **14th Eur. PV Solar Energy Conf.**, 157-160 (1997).
5. P. Ho and J. Gee, **Thermochemical Analysis for Purification of Polysilicon Melts**, Sandia National Laboratories Report, SAND99-1047, May 1999.
6. R. J. Kee, R. M. Rupley, and J. A. Miller, "The Chemkin Thermodynamic Data Base," Sandia National Laboratories Report No. **SAND87-8215B**, March 1990. http://www.ran.sandia.gov/chemkin/
7. B. McBride, S. Gordon, and M. Reno, "CET/93PC, Chemical Equilibrium with Transport Properties," NASA Lewis Research Center, 1993. Available from COSMIC, the NASA Software Technology Transfer Center. http://www.ran.sandia.gov/chemkin/
8. Private communication, John Noring, Lawrence Livermore National Laboratory. http://www.ran.sandia.gov/chemkin/
9. M. W. Chase, Jr., C. A. Davies, J. R. Downey, Jr., D. J. Frurip, R. A. McDonald, A. N. Syverud, JANAF Thermochemical Tables, 3rd edition, **J. Phys. Chem. Ref. Data, 14**, *Supp. 1*, (1985). http://www.ran.sandia.gov/chemkin/
10. **Handbook of Chemistry and Physics, 52nd edition**, Robert C. Weast, Editor, The Chemical Rubber Company, Cleveland, 1971.
11. C. P. Khattak, and F. Schmid, "Processing of MG Silicon for Photovoltaic Applications," in **Proceedings of the Symposium on Materials and New Processing Technologies for Photovoltaics**, J.A. Mick, V. K. Kapur and J. Dietl, Eds., Proceedings Volume 83-11, The Electrochemical Society, Pennington, NJ, 478-489 (1983).
12. V.D. Dosaj, L.P. Hunt, and L.D. Crossman, "Single crystal silicon ingot pulled from chemically-upgraded metallurgical-grade silicon," **11th IEEE Photo. Spec. Conf.**, 275-279 (1975).
13. L.P. Hunt, V. D. Dosaj, J. R. McCormick, and L. D. Crossman, "Production of solar-grade silicon from purified metallurgical silicon," **12th IEEE Photo. Spec. Conf.**, 125-129 (1977).
14. Y. Sakaguchi, N. Yuge, N. Nakamura, H. Baba, K. Hanazawa, M. Abe and Y. Kato, "Purification of metallic grade silicon up to solar grade by NEDO melt purification process," **14th Eur. PV Solar Energy Conf.**, 157-160 (1997).

DISTRIBUTION

Dr. Chandra Khattak
Crystal Systems, Inc.
27 Congress Street
Salem, MA 01970

Dr. Bob Hall
AstroPower
Solar Park
Newark, DE 19716-2000

Dr. James Rand
AstroPower
Solar Park
Newark, DE 19716-2000

Dr. Frank Zanner
80 Skyline Drive
Sandia Park, NM 87047

Dr. Richard King
U.S. Department of Energy
Forrestal Bldg., EE-11
1000 Independence Ave., SW
Washington, DC 20585

Dr. Jeffrey Mazer
U.S. Department of Energy
Forrestal Bldg., EE-11
1000 Independence Ave., SW
Washington, DC 20585

Mr. Ted Ciszek
National Renewable Energy Lab
1617 Cole Blvd.
Golden, CO 80401-3393

Dr. Tihụ Wang
National Renewable Energy Lab
1617 Cole Blvd.
Golden, CO 80401-3393

Dr. Bhushan Sopori
National Renewable Energy Lab
1617 Cole Blvd.
Golden, CO 80401-3393

Dr. Mohan Narayanan
Solarex Corporation
630 Solarex Court
Frederick, MD 21701

Dr. John Wohlgemuth
Solarex Corporation
630 Solarex Court
Frederick, MD 21701

Ed Henderson
Matrix Solar
P. O. Box 14740
Albuquerque, NM 87191-4740

Ron Gehringer
SiNaF Products, Inc.
5600 Gibson Blvd. SE
Bldg. 153
Albuquerque, NM 87108

Dr. Jack Hanoka
Evergreen Solar, Inc.
211 Second Avenue
Waltham, MA 02154

Dr. Andrew Gabor
Evergreen Solar, Inc.
211 Second Avenue
Waltham, MA 02154

Dr. Juris Kalejs
ASE Americas, Inc.
Four Suburban Park
Billerica, MA 01821-3980

Dr. Mark Rosenblum
ASE Americas, Inc.
Four Suburban Park
Billerica, MA 01821-3980

Ms. Theresa Jester
Siemens Solar Industries
P. O. Box 6032
Camarillo, CA 93011

Dr. Dan Meier
Ebara Solar, Inc.
811 Route 51 South
Large, PA 15025

Prof. Ajeet Rohatgi
Georgia Institute of Technology
777 Atlantic Drive
School of Electrical Engineering
Atlanta, GA 30332

Dr. G. Mihalik
Siemens Solar Industries
12016 N.E. 95th Street
Suite 720
Vancouver, WA 98682

Gary Stevens
Matrix Solar
7500 Meridian Place
Albuquerque, NM 87121

0601 Pauline Ho, 1126
0601 Jeff Tsao, 1126
0752 James Gee, 6219
(10 copies)
0752 Dan Aiken, 6219
0752 David King, 6219
0752 Doug Ruby, 6219
0753 Chris Cameron, 6218
0753 PV Library, 6218
(10 copies)
1134 James Van den Ayvle, 1846
1203 John M. Taylor, 5335
1349 Richard J. Salzbrenner, 1846
9018 Central Tech Files, 8940-2
0899 Technical Library, 9619
(2 copies)
0612 Review & Approval Desk,
9612, for DOE/OSTI